

Hierarchical Control of State Transitions in Dense Associative Memories

Anton Grishechkin, Abhirup Mukherjee, and Omer Karin

Department of Mathematics, Imperial College London, London, SW7 2AZ, UK

We analyze a generalization of Modern Hopfield networks that emerges naturally in the gene regulatory networks that control cellular identity. Here gene expression patterns correspond to stored memories and the dynamics are governed by the interplay between an inverse-temperature-like parameter β and a weight vector \mathbf{w} . The parameter β controls the attractor landscape structure: at large β , memory patterns are stable attractors, while at lower β values, the attractors are associated with progenitor patterns—weighted combinations of two or more memory patterns. We associate progenitor states with self-similarity of the model following a coarse-graining transformation on memory pattern subsets. We use this transformation to propose a hierarchical model for the control of the identity, stability, and basins of attraction of the progenitor states which facilitates transitions between memory patterns through an annealing-like mechanism. We use this framework to explain the dynamical regulation of blood formation in mammals, demonstrating how robust control of attractor transitions may emerge in complex feedback networks and providing a mathematical basis for well-established experimental observations on the hierarchical control of cell identity.

Introduction - The challenge of understanding how complex biological systems can store and retrieve memories has been a subject of intense study since Hopfield's groundbreaking work on attractor networks [1, 2]. Classical Hopfield networks relied on pairwise interactions between nodes, with interaction strength determined by Hebb's rule. While these networks were conceptually striking as models for brain function, they had major limitations, such as limited storage capacity and the inability to store correlated patterns. More recent work demonstrated that exponential storage capacity can be achieved through higher-order interactions [3–7]. These networks are known as Dense Associative Memories or Modern Hopfield networks.

Cell identity behavior in animals exhibits many qualitative similarities to associative memory networks [8, 9]. Different cell types in an animal have unique gene expression profiles that remain stable throughout its life. These profiles correspond to the 'memory patterns' of the gene regulatory network. Dynamic retrieval of these expression patterns is crucial during differentiation processes, such as during development or in the self-renewal of adult tissues from stem populations. Additionally, experimental perturbations, such as artificially over-expressing specific genes, can reprogram between distinct cell types. Reprogramming shares qualitative similarities with the recall of associative memories, and computational models based on Hopfield networks have successfully predicted the effects of reprogramming perturbations [8, 10, 11]. However, the mechanistic implementation of these networks within cells remained unclear.

We recently proposed that a generalization of Modern Hopfield networks emerges naturally in the gene regulatory networks that control cell identity [11]. These networks are dominated by feedback interactions between proteins called transcription factors (TFs) that bind DNA regions known as enhancers. Each enhancer is associated with a unique TF binding profile; TF binding leads to the recruitment of specific enzymes, called cofactors, which modulate enhancer chromatin, which, in turn,

determines the rate at which transcription initiation machinery is recruited to the enhancer [12, 13]. This results in the following gene expression dynamics, taking equilibrium recruitment of transcriptional machinery on the timescale of cell identity changes, and with time rescaled to unity:

$$\dot{\mathbf{x}} = g(\mathbf{x}, \beta, \mathbf{Q}, \Xi, \mathbf{w}) = \mathbf{Q}^T \text{softmax}(\beta \Xi \mathbf{x} + \mathbf{w}) - \mathbf{x} \quad (1)$$

where \mathbf{x} is the gene expression vector and Ξ is the matrix whose K rows correspond to physical enhancer binding profiles, that is, the affinity of the enhancer to each of the N TFs. \mathbf{Q} is a matrix associating each enhancer with its effect on the expression of each of the TFs, and β is an inverse-temperature-like scalar associated with the turnover of chromatin modifications. The weight vector \mathbf{w} is the baseline enhancer activity and can be modulated by upstream signalling or persistent DNA and chromatin modifications, and softmax is the Boltzmann distribution. As we will show, the parameter β controls plasticity - the range of gene expression patterns accessible to the dynamics, while \mathbf{w} biases specific patterns.

Eq. 1 is similar to the Continuous Modern Hopfield network update rule presented in [6], except that there, $\mathbf{w} = \mathbf{0}$ and $\mathbf{Q} = \Xi$. In [11] we showed that a recurring motif in cell identity networks, where sets of TFs co-bind their own enhancers, implies that Eq. 1 can be approximated by a symmetric form:

$$\dot{\mathbf{x}} = \Xi^T \text{softmax}(\beta \Xi \mathbf{x} + \mathbf{w}) - \mathbf{x} \quad (2)$$

where now the rows of Ξ are set by the observed gene expression patterns of different cell types. The symmetric dynamics are associated with gradient descent along an energy (potential) function:

$$\dot{\mathbf{x}} = -\nabla V(\mathbf{x}, \beta, \Xi, \mathbf{w}) \quad (3)$$

with $V(\mathbf{x}, \beta, \Xi, \mathbf{w}) = -\beta^{-1} \log Z + \frac{1}{2} \mathbf{x}^T \mathbf{x}$, where Z is the normalizing constant of softmax in Eq. 2. The dynamics specified by Eq. 2 quantitatively recapitulate key aspects

of cell identity regulation, including reprogramming and hierarchical differentiation [11]. Eq. 2 successfully predicts the reprogramming effects of the over-expression of specific sets of genes. It also predicts the complex differentiation landscape of blood formation through a simple annealing mechanism based on a decrease in β , which destabilizes the stem cell state, followed by an increase in β that results in differentiation [11].

The success of Eq. 2 in capturing high-dimensional differentiation and reprogramming dynamics, and its relevance to a wide range of applications in neuroscience, cell biology, and machine learning [6, 14, 15], provides strong motivation for developing a theoretical understanding of its dynamics. Here we focus on understanding how it can support robust control of transitions between attractor states through the annealing mechanism. We show that decreasing β coarsens the dynamics of Eq. 2 into a self-similar form associated with multiple progenitor patterns corresponding to weighted combinations of subsets of patterns of Ξ . Each progenitor pattern is associated with a persistence length of β , set by the maximal angle between any of its constituent patterns, for which it corresponds to an effective pattern in the dynamics. We use self-similarity to demonstrate that modulation of \mathbf{w} allows controlling identity transitions between memory pattern states during annealing by adjusting the composition and basins of attraction of progenitor and descendant patterns, providing a robust mechanism for hierarchical control that recapitulates the dynamics of blood formation.

Coarse-graining by self-similarity. The analysis hereafter considers patterns (rows of Ξ) of equal magnitude; a straightforward generalization to patterns of unequal magnitude is provided in the appendix. This magnitude is assumed without loss of generality to be unity (otherwise model parameters can be rescaled appropriately). We first show that the dynamics of the model are self-similar and that the inverse temperature β coarse-grains the dynamics in a hierarchical manner. Consider a subset of indices $\mathcal{L} \subseteq \{1 \dots K\}$ and denote the transformation $\mathbf{Q} \xrightarrow{\mathcal{L}} \mathbf{Q}', \Xi \xrightarrow{\mathcal{L}} \Xi', \mathbf{w} \xrightarrow{\mathcal{L}} \mathbf{w}'$, where $\mathbf{Q}' = \mathbf{Q}_{i \notin \mathcal{L}} \cup \{Q_{\mathcal{L}}^*\}$, $\Xi' = \Xi_{i \notin \mathcal{L}} \cup \{\Xi_{\mathcal{L}}^*\}$, $\mathbf{w}' = \mathbf{w}_{i \notin \mathcal{L}} \cup \{w_{\mathcal{L}}^*\}$, with:

$$\begin{aligned} Q_{\mathcal{L}}^* &= \frac{\sum_{i \in \mathcal{L}} Q_i e^{w_i}}{\sum_{i \in \mathcal{L}} e^{w_i}} \\ \Xi_{\mathcal{L}}^* &= \frac{\sum_{i \in \mathcal{L}} \Xi_i e^{w_i}}{\sum_{i \in \mathcal{L}} e^{w_i}} \\ w_{\mathcal{L}}^* &= \log \sum_{k \in \mathcal{L}} e^{w_k} \end{aligned} \quad (4)$$

where Q_i is the i -th row of \mathbf{Q} , Ξ_i is the i -th row of Ξ , and w_i is the i -th element of \mathbf{w} . The transformation coarse-grains the dynamics as the patterns and weights associated with the transformed dynamics are weighted averages of the original patterns. We refer to $\Xi_{\mathcal{L}}^*$ as the *progenitor pattern* associated with \mathcal{L} .

We make the following mathematical observations on the transformation. First, sequential applications of the transformation on disjoint subsets of indices in a set are equivalent to a single application on the entire set. We therefore refer to the transformed dynamics as $g_{\mathcal{L}}(\mathbf{x}, \beta, \mathbf{Q}, \Xi, \mathbf{w})$ and refer to the transformed potential (if it exists) as $V_{\mathcal{L}}(\mathbf{x}, \beta, \Xi, \mathbf{w})$. Second, the transformation preserves symmetry, that is, if $\Xi_i = Q_i$ for all $i \in \mathcal{L}$ then $Q_{\mathcal{L}}^* = \Xi_{\mathcal{L}}^*$. And third, if the rows $\Xi_i, i \in \mathcal{L}$ are identical then the transformation leaves the dynamics unchanged; that is, when $\Xi_i = \Xi_k$ for $i, k \in \mathcal{L}$ then $g_{\mathcal{L}}(\mathbf{x}, \beta, \mathbf{Q}, \Xi, \mathbf{w}) = g(\mathbf{x}, \beta, \mathbf{Q}, \Xi, \mathbf{w})$, and, in the symmetric case, $V_{\mathcal{L}}(\mathbf{x}, \beta, \Xi, \mathbf{w}) = V(\mathbf{x}, \beta, \Xi, \mathbf{w})$.

The last observation can be extended by considering the effect of the transformation on non-identical patterns. Consider two patterns Ξ_i, Ξ_k and let $\theta = \phi, \theta + \phi, \mu_{i,k}$ denote $\angle(\Xi_i, \mathbf{x}), \angle(\Xi_k, \mathbf{x}), \angle(\Xi_i, \Xi_k)$, noting that from the triangle inequality of angles we have that $\phi \leq \mu_{i,k}/2$. Expanding to a second order in ϕ :

$$V_{\mathcal{L}}(\mathbf{x}, \beta, \Xi, \mathbf{w}) \approx V(\mathbf{x}, \beta, \Xi', \mathbf{w}') + \|\mathbf{x}\|^2 \nu \beta \phi^2 \sin^2(\theta) \quad (5)$$

with $\nu < 1/2$, and thus the correction term is of magnitude at most $\frac{1}{8} \beta \mu_{i,k}^2$ (note that, in general, \mathbf{x} is contained within the convex hull spanned by Ξ and thus $\|\mathbf{x}\| \leq 1$). Thus, when the inverse temperature β is sufficiently small compared with $\mu_{i,k}^2$, the transformed dynamics are effectively identical to Eq. 3 with the coarse-grained pattern $\Xi_{i,k}^*$ replacing patterns i, k (Figure 1). Now, let us assume that the patterns are isolated, that is, $\mu_{i,k}$ is small compared to the angles $\mu_{i,l}, \mu_{k,l}$ for $l \neq i, k$, and consider the dynamics in the vicinity of the coarse-grained pattern $\Xi_{i,k}^*$ for $\beta \approx \mu_{i,k}^{-2}$. In this case the other patterns make negligible contributions to the dynamics and the dynamics reduce to two-pattern effective dynamics; in this case, there is a bifurcation at $\beta_{\text{crit}} = 4\mu_{i,k}^{-2}$ where the progenitor $\Xi_{i,k}^*$ is destabilized, leading to the stabilization of Ξ_i, Ξ_k . More generally, in the case of $|\mathcal{L}|$ patterns that are of similar angle μ with each other, we have that the pattern $\Xi_{\mathcal{L}}^*$ is destabilized at $\beta_{\text{crit}} = 2|\mathcal{L}|\mu^{-2}$. For patterns of unequal angle, the correction term depends on the largest angle in the set $\mu_{\mathcal{L}}$,

$$V_{\mathcal{L}}(\mathbf{x}, \beta, \Xi, \mathbf{w}) \approx V(\mathbf{x}, \beta, \Xi', \mathbf{w}') + O(\beta \mu_{\mathcal{L}}^2) \quad (6)$$

Where the correction term is at most $\frac{1}{4} \beta \mu_{\mathcal{L}}^2$. The progenitor $\Xi_{\mathcal{L}}^*$ thus has a *persistence length* which depends on the statistical structure of the associated patterns $\Xi_{i \in \mathcal{L}}$ and is of order $\mu_{\mathcal{L}}^{-2}$. This suggests a hierarchical self-similar coarsening of the dynamics with decreasing β . Specific patterns are attractors at large β , while, as β decreases, these patterns destabilize and are replaced by stable progenitor patterns. As β decreases further, these progenitors may themselves destabilize and be replaced by other stable progenitors associated with larger subsets of patterns, with the transitions set by the persistence lengths of the various subsets.

The coarse-graining transformation can be applied to overlapping sets, whose persistence lengths can be distinct. For example, two overlapping pairs of patterns

may be similar $\angle(\Xi_i, \Xi_k) = \mu, \angle(\Xi_i, \Xi_l) = \mu$, while the third pair is less similar $\angle(\Xi_l, \Xi_k) = 2\mu$, and the persistence length of the progenitor of Ξ_l, Ξ_k is much shorter than that of the progenitor of Ξ_i, Ξ_k and that of Ξ_i, Ξ_l . Finally, while the persistence length can capture precisely patterns of stabilization and destabilization of progenitors in strictly hierarchical sets of patterns with strong separation in pattern similarities, in other cases more complex stability properties can emerge, such as meta-progenitors that arise from recursive applications of the transformation to overlapping progenitor states. Nevertheless, by Eq. 4, a subset of patterns \mathcal{L} become coupled through their progenitor $\Xi_{\mathcal{L}}^*$ for values of β smaller than their persistence length.

Hierarchical control of basins of attraction and progenitor identity. We next consider the effect of modulation of the \mathbf{w} vector on the dynamics. We can see from the transformation given by Eq. 4 that a change in w_i , the weight entry associated with pattern i , modulates the pattern associated with each progenitor $\Xi_{\mathcal{L}}^*$ where $i \in \mathcal{L}$ (for $|\mathcal{L}| \geq 2$). These progenitors are modulated in such a way that the relative contribution of Ξ_i to $\Xi_{\mathcal{L}}^*$ increases and thus the similarity between Ξ_i and $\Xi_{\mathcal{L}}^*$ increases. All other progenitors and patterns, including Ξ_i itself, are not affected. Thus \mathbf{w} modulates progenitor identity in a hierarchical manner.

We next analyzed the effect of \mathbf{w} modulation on the basins of attraction of patterns and progenitors. In general, for a pattern Ξ_i that is a stable fixed point, an increase in w_i decreases its associated energy $V(\Xi_i)$, with a small increase having a negligible effect on the ener-

gies of all other stable patterns. This effect results in an increase in the basin of attraction of pattern i , at the expense of competing patterns. As an example, consider two competing patterns Ξ_i, Ξ_k with $\angle(\Xi_i, \Xi_k) = \mu$ and with $\beta \gg \beta_{\text{crit}}$. For a small $w_i - w_k$ the offset of the separatrix from the mid-way point between the patterns is given by $\Delta = -\frac{(w_i - w_k) \sin(\frac{\mu}{2})}{\beta(1 - \cos(\mu))}$ and thus the basin of attraction increases in proportion to the weight difference. Our analysis similarly extends to progenitor states associated with Ξ_i , with their basins of attraction also increasing with w_i .

Annealing. The modulation of w_i has opposite effects on progenitor identity and on the basin of attraction of Ξ_i . While the basin of attraction of Ξ_i increases with w_i , that is, Ξ_i is attractive from a wider range of states, the identities of progenitors associated with Ξ_i become more similar to Ξ_i ; at an extreme, for sufficiently large w_i , the basin of attraction of Ξ_i encompasses all of the convex hull spanned by Ξ , while the progenitors are all identical to Ξ_i . Thus, modulation of w_i changes the likelihood that a progenitor of Ξ_i will be within its basin of attraction.

Self-similarity allows us to extend this observation in a hierarchical manner. Starting from a large β where Ξ_i is a stable fixed point and decreasing β , the pattern Ξ_i may coarsen into various progenitors, which, as β decreases further, may themselves coarsen into other progenitors, until, ultimately, all patterns coarsen into $\mathbf{x} = \Xi^T \text{softmax}(\mathbf{w})$. Consider, for example, an initial coarsening of Ξ_i to $\Xi_{\mathcal{L}_1}^*$ followed by a coarsening into $\Xi_{\mathcal{L}_2}^*$ (we therefore have that $i \in \mathcal{L}_1, \mathcal{L}_1 \subset \mathcal{L}_2$). An increase in w_i leads to an increase in the basins of attractions of all progenitor patterns, due to an increase in their associated weights, and increases their similarity compared with competing patterns that do not incorporate Ξ_i . Thus, an increase in w_i increases the likelihood that decoarsening (increasing β) will proceed through Ξ_i -associated progenitors.

The observation on how \mathbf{w} controls progenitor identity and basins of attraction suggests that an annealing mechanism, whereby β is decreased, and then slowly increased, can be used to transition between attractor states (Figure 2). Namely, modulation of \mathbf{w} can control the end states of the annealing process. In the presence of noise or variability in parameters, an increase in w_i can increase the *rate* at which pattern Ξ_i is formed. A feedback controller that adjusts w_i according to the production rate of different patterns can thus allow control over the fraction of patterns produced.

Application to gene regulatory networks and blood formation. We now apply the theoretical framework to the processes of cell identity regulation in animals, focusing on the dynamics of blood formation. Recall that in this context, \mathbf{x} corresponds to TF expression, the rows of Ξ correspond to the binding patterns of physical enhancers, and \mathbf{Q} corresponds to the effect of these enhancers on gene expression. Cellular differentiation proceeds through the activation of specific sets of enhancers [16], which, in the model, corresponds to high level of

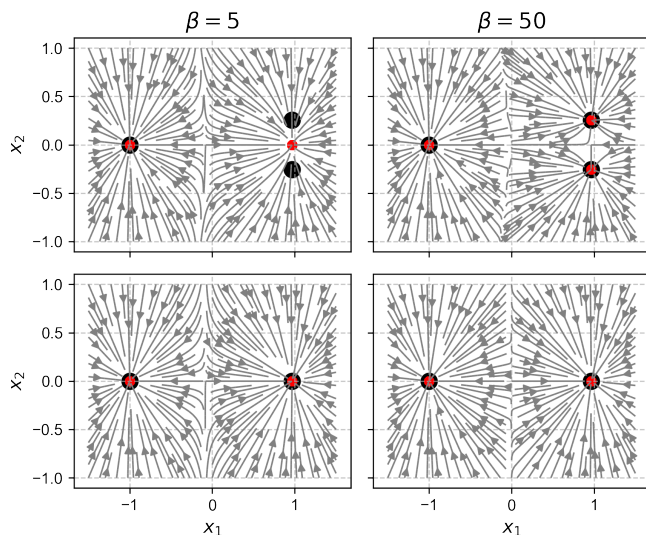


FIG. 1. Stream plots, patterns (black) and stable steady-states (red) for the dynamics given by Eq. 2 and parameterized with $\mathbf{w} = \mathbf{0}$ (upper panels) or the dynamics where the two patterns associated with positive x_1 are coarse-grained by Eq. 4 (lower panels). Coarse-graining is accurate for $\beta \ll \beta_{\text{crit}}$ (here $\beta_{\text{crit}} = 15$) but fails for $\beta > \beta_{\text{crit}}$.

activity (large softmax entries) associated with specific rows of Ξ . We therefore expect that these rows represent stable attractor states of the dynamics. However, the dynamics of Eq. 1 are general and the patterns Ξ need not a-priori correspond to attractor states. To arrive at the symmetric dynamics, we use a crucial experimental observation - that, across cell types, the TFs that control cell identity form dense autoregulatory networks where they co-bind cell-type-specific enhancers [17]. Within our modelling framework, these autoregulatory networks correspond to a subset \mathcal{L} of enhancers and a subset \mathcal{M} of TFs such that the enhancers in $\Xi_{i \in \mathcal{L}}$ have similar binding patterns associated with \mathcal{M} , while their activation vectors $Q_{i \in \mathcal{L}}$ each have a positive entry associated with a TF in \mathcal{M} . The application of the transformation Eq. 4 will in this case leave the dynamics unchanged, resulting in symmetric patterns $Q_{\mathcal{L}}^* \approx \Xi_{\mathcal{L}}^*$. Repeated application of the transformation to all autoregulatory circuits will thus recover symmetric dynamics with specific autoregulatory circuits acting as potential attractor patterns, in line with experimental knowledge. Thus, autoregulation implies that Eq. 1 can be coarse-grained such that the corresponding rows of \mathbf{Q} and Ξ are correlated.

Both \mathbf{Q} and Ξ are in principle observable as they relate to TF expression and TF binding; however \mathbf{Q} is more readily interpretable as it can be inferred directly from widely available gene expression data. The symmetry in the dynamics implies that it is possible to approximate Ξ as $\Xi = \mathbf{Q}$ and thus approximate the entire dynamics from observed expression patterns, leaving only the weight \mathbf{w} and plasticity β as free parameters. This approximation can successfully predict the effect of reprogramming by the constitutive expressions of specific TFs [11], which corresponds to specific perturbations to \mathbf{w} directed by the association matrix Ξ .

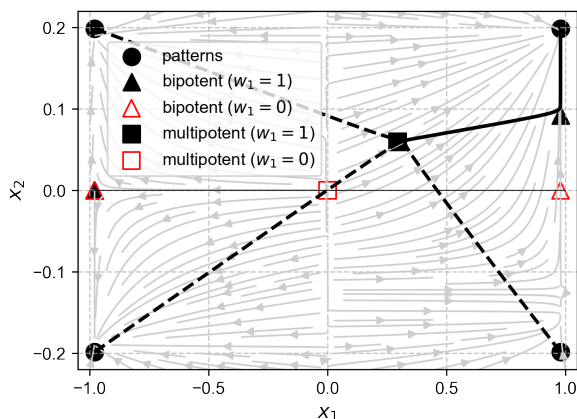


FIG. 2. Annealing trajectory (black lines) of Eq. 2 for a set of 4 patterns, where for the upper right pattern $w_1 = 1$ while for others $w_2 = w_3 = w_4 = 0$; on the background are the stream lines at $\beta = 50$ for $w_1 = 1$. The dashed segments represent the transition to the multipotent progenitor state in the annealing process.

While modulating \mathbf{w} by itself allows transitions between attractor states, it does so by destroying the attractor landscape and thus does not provide a plausible model for controlled transitions where multiple attractor states need to co-exist, such as in gene regulatory networks that need to support a range of stem and differentiated cellular states. However, the combination of annealing and feedback control of \mathbf{w} can robustly transition the dynamics between attractor states, as we demonstrate for blood formation (Figure 3). Here, as in Karin [11], we set the rows of Ξ as the averaged expression patterns for the 11 major blood lineages, and consider the dynamics of annealing for blood lineages in the presence of noise which allows for distinct outcomes in the annealing process. We also set \mathbf{w} through proportional negative feedback, simulating negative feedback on cellular production in the body [18, 19]. This results in balanced differentiation into all fates, through a bifurcating differentiation landscape (Figure 3A,B). An increase in w_i increases the rate of production of lineage i through an increase in the contribution of its expression pattern to progenitor states. We demonstrate this by increasing the \mathbf{w} entry associated with the erythrocyte fate (Figure 3C,D) which increases both the production rate of erythrocytes and the relative contribution of the erythrocyte expression profile to its associated progenitor states, recapitulating the effect of erythropoietin on red blood cell production [20] (Figure 3). The identity of progenitor states and their persistence lengths are captured by our theoretical framework (Figure 3E).

Crucially, the structure of the differentiation landscape can be predicted from the persistence lengths of the different progenitor states (Figure 3E,F). Blood progenitors and their differentiation potential have been extensively characterized through a variety of experimental approaches, including in-vitro culture assays, transplantation studies, single-cell gene expression and chromatin analysis, and fate mapping [22, 23]. While, in principle, many possible progenitor sets may appear ($2^{11} = 2048$), much fewer progenitors are observed, including progenitors with overlapping differentiation potential which can provide alternative differentiation routes to the same fate. This raises the question of why these specific sets of progenitors and differentiation routes are observed. The model predicts that (a) progenitors with longer persistence lengths compared with competing progenitor states are more likely to be observed, as they can represent attractor states for a wider range of β values during the annealing process; and (b), between competing progenitor states with similar persistence lengths, those that incorporate a wider range of terminal states are more likely to be observed as they have larger associated emergent \mathbf{w} entries. To test whether this can explain the observed progenitor states in blood formation, we plotted the computed persistence lengths of all possible progenitor states (Figure 3F), with observed progenitor states (reviewed in [22, 24]) plotted as pie charts with a black circumference according to their composition; more recently

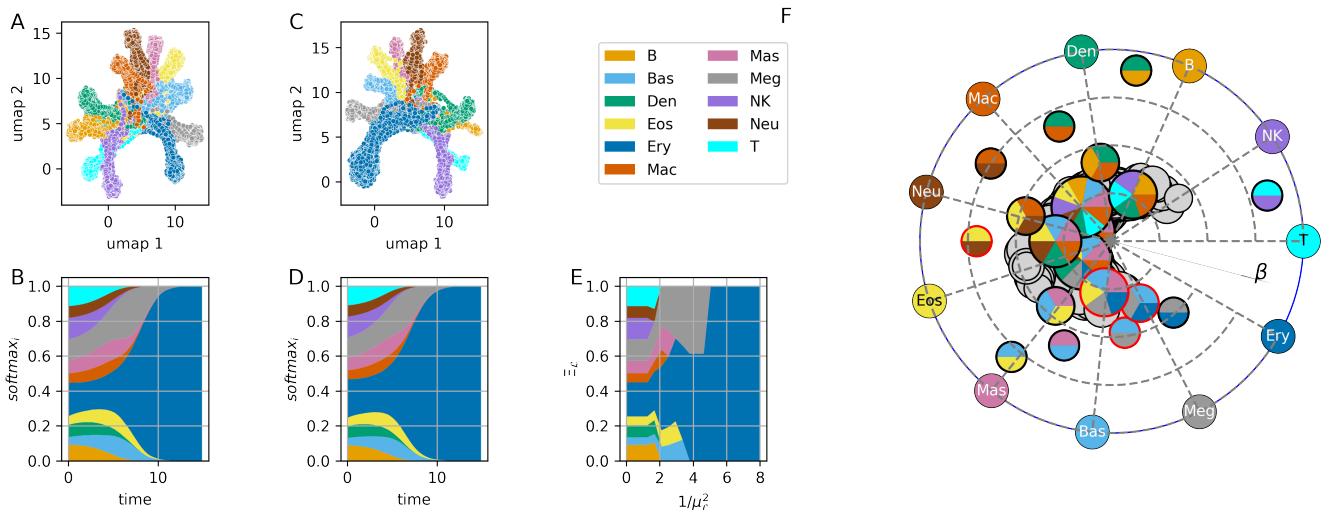


FIG. 3. **Annealing and the dynamics of blood formation.** The matrix Ξ was initialized from the averaged mouse gene expression profiles of 11 major blood lineages from Haemopedia [21], initialized as in Karin [11]. (A-D) Simulations of annealing on hematopoietic lineages, with \mathbf{w} set by a proportional negative feedback controller with an error proportional to the imbalance of blood cell production (A,B), and with the entry associated with erythrocytes (red blood cells) increased by 20% in (C,D). In all simulations the noisy version of Eq. 1 was used (Appendix). (A,C) Annealing trajectories were plotted using Uniform Manifold Approximation and Projection (UMAP) and colored by terminal cell type. (B,D) average contribution of different blood lineage expression programs to $\mathbf{x}(t)$ during annealing that results in erythrocytes, given by $\text{softmax}(\beta \Xi \mathbf{x} + \mathbf{w})$. (E) Heuristic prediction of progenitor states during an annealing process that results in erythrocyte differentiation. At each persistence length the largest progenitor state that is associated with an erythrocyte lineage is selected and plotted according to the relative contributions of each blood lineage to its expression profile, given by the transformation Eq. 4. Simulation parameters are provided in the Appendix. (F) Progenitor states were plotted at a radius proportional to their corresponding persistence length, set by $1/\mu_L^2$.

discovered basophil/megakaryocyte/erythrocyte progenitors [25, 26], as well as a eosinophilic/neutrophilic progenitor [27–29] were plotted with red circumference; and unobserved states were plotted as grey dots. The observed restricted potential progenitors have longer persistence lengths compared with their competitors, while, at smaller values of β , multipotent progenitor states predominate (Figure 3F). We can therefore quantitatively predict the simulated and experimentally observed progenitor states through persistence length quantification.

The dynamics of differentiation in our model exhibit both similarities and differences compared to Waddington’s classic epigenetic landscape picture of cellular differentiation [9, 30, 31]. As in the Waddingtonian picture, differentiation in the annealing model proceeds in a hierarchical manner through a series of bifurcations, from multipotent to ever more restricted progenitors. The modelling framework presented here makes the concept of potency quantitatively precise, in that we show that a differentiation signal for fate i , which modulates w_i ,

will perturb all progenitors associated with this fate towards it; while other progenitors will not be affected. Our analysis thus unifies the experimental observations on hierarchical differentiation, multilineage priming, and differentiation potency, into a single mathematical framework. In contrast to the classical Waddingtonian picture, however, our hierarchical picture does not entail tree-like differentiation landscape. Rather, analysis suggests that differentiation landscapes may be much more flexible, with multiple possible pathways to the same target fate; moreover, the pathways taken may themselves change according to signaling which can lead to changes in the basins of attraction of the progenitor states. These flexible and non-tree like dynamics are in line with experimental knowledge on complex differentiation dynamics in systems such as blood formation and neural crest differentiation [22, 32]. While our analysis proposes flexible differential landscapes, these landscapes are nevertheless constrained by the statistical structure of the target states and can be quantitatively predicted through the persistence length measure.

[1] J. J. Hopfield, Neural networks and physical systems with emergent collective computational abilities., Proceedings

of the national academy of sciences **79**, 2554 (1982).
[2] D. J. Amit, H. Gutfreund, and H. Sompolinsky, Storing

- infinite numbers of patterns in a spin-glass model of neural networks, *Physical Review Letters* **55**, 1530 (1985).
- [3] D. Krotov and J. J. Hopfield, Dense associative memory for pattern recognition, *Advances in neural information processing systems* **29** (2016).
- [4] M. Demircigil, J. Heusel, M. Löwe, S. Upgang, and F. Vermet, On a model of associative memory with huge storage capacity, *Journal of Statistical Physics* **168**, 288 (2017).
- [5] D. Krotov and J. Hopfield, Large associative memory problem in neurobiology and machine learning, arXiv preprint arXiv:2008.06996 (2020).
- [6] H. Ramsauer, B. Schäfl, J. Lehner, P. Seidl, M. Widrich, T. Adler, L. Gruber, M. Holzleitner, M. Pavlović, G. K. Sandve, *et al.*, Hopfield networks is all you need, arXiv preprint arXiv:2008.02217 (2020).
- [7] C. Lucibello and M. Mézard, Exponential capacity of dense associative memories, *Physical Review Letters* **132**, 077301 (2024).
- [8] A. H. Lang, H. Li, J. J. Collins, and P. Mehta, Epigenetic landscapes explain partially reprogrammed cells and identify key reprogramming genes, *PLoS computational biology* **10**, e1003734 (2014).
- [9] N. E. Boukacem, A. Leary, R. Thériault, F. Gottlieb, M. Mani, and P. François, Waddington landscape for prototype learning in generalized hopfield networks, *Physical Review Research* **6**, 033098 (2024).
- [10] S. T. Pusuluri, A. H. Lang, P. Mehta, and H. E. Castillo, Cellular reprogramming dynamics follow a simple 1d reaction coordinate, *Physical Biology* **15**, 016001 (2017).
- [11] O. Karin, Enhancernet: A predictive model of cell identity dynamics through enhancer selection, *Development* **151**, dev202997 (2024).
- [12] T. Narita, S. Ito, Y. Higashijima, W. K. Chu, K. Neumann, J. Walter, S. Satpathy, T. Liebner, W. B. Hamilton, E. Maskey, *et al.*, Enhancers are activated by p300/cbp activity-dependent pic assembly, rnapii recruitment, and pause release, *Molecular Cell* **81**, 2166 (2021).
- [13] J. J. Ferrie, J. P. Karr, T. G. Graham, G. M. Dailey, G. Zhang, R. Tjian, and X. Darzacq, p300 is an obligate integrator of combinatorial transcription factor inputs, *Molecular Cell* **84**, 234 (2024).
- [14] L. Ambrogioni, In search of dispersed memories: Generative diffusion models are associative memory networks, arXiv preprint arXiv:2309.17290 (2023).
- [15] E. Spens and N. Burgess, A generative model of memory construction and consolidation, *Nature Human Behaviour* **8**, 526 (2024).
- [16] D. Hnisz, B. J. Abraham, T. I. Lee, A. Lau, V. Saint-André, A. A. Sigova, H. A. Hoke, and R. A. Young, Super-enhancers in the control of cell identity and disease, *Cell* **155**, 934 (2013).
- [17] V. Saint-André, A. J. Federation, C. Y. Lin, B. J. Abraham, J. Reddy, T. I. Lee, J. E. Bradner, and R. A. Young, Models of human core transcriptional regulatory circuitries, *Genome research* **26**, 385 (2016).
- [18] A. Stanoev and A. Koseska, Robust cell identity specifications through transitions in the collective state of growing developmental systems, *Current Opinion in Systems Biology* **31**, 100437 (2022).
- [19] B. D. Simons and O. Karin, Tuning of plasma cell lifespan by competition explains the longevity and heterogeneity of antibody persistence, *Immunity* **57**, 600 (2024).
- [20] A. Grover, E. Mancini, S. Moore, A. J. Mead, D. Atkinson, K. D. Rasmussen, D. O’Carroll, S. E. W. Jacobsen, and C. Nerlov, Erythropoietin guides multipotent hematopoietic progenitor cells toward an erythroid fate, *Journal of Experimental Medicine* **211**, 181 (2014).
- [21] J. Choi, T. M. Baldwin, M. Wong, J. E. Bolden, K. A. Fairfax, E. C. Lucas, R. Cole, C. Biben, C. Morgan, K. A. Ramsay, *et al.*, Haemopedia rna-seq: a database of gene expression during haematopoiesis in mice and humans, *Nucleic acids research* **47**, D780 (2019).
- [22] R. Ceredig, A. G. Rolink, and G. Brown, Models of haematopoiesis: seeing the wood for the trees, *Nature Reviews Immunology* **9**, 293 (2009).
- [23] E. Laurenti and B. Göttgens, From hematopoietic stem cells to complex differentiation landscapes, *Nature* **553**, 418 (2018).
- [24] G. Brown and I. Sanchez-Garcia, Is lineage decision-making restricted during tumoral reprogramming of hematopoietic stem cells?, *Oncotarget* **6**, 43326 (2015).
- [25] A. Wanet, M. A. Bassal, S. B. Patel, F. Marchi, S. A. Mariani, N. Ahmed, H. Zhang, M. Borchiellini, S. Chen, J. Zhang, *et al.*, E-cadherin is regulated by gata-2 and marks the early commitment of mouse hematopoietic progenitors to the basophil and mast cell fates, *Science immunology* **6**, eaba0178 (2021).
- [26] J. Park and S.-J. Kang, The ontogenesis and heterogeneity of basophils, *Discovery Immunology* **3**, kyae003 (2024).
- [27] D. Metcalf, S. Mifsud, and L. Di Rago, Stem cell factor can stimulate the formation of eosinophils by two types of murine eosinophil progenitor cells, *Stem Cells* **20**, 460 (2002).
- [28] K. Kim, S. M. Hwang, S. M. Kim, S. W. Park, Y. Jung, and I. Y. Chung, Terminally differentiating eosinophils express neutrophil primary granule proteins as well as eosinophil-specific granule proteins in a temporal manner, *Immune Network* **17**, 410 (2017).
- [29] I. Kwok, E. Becht, Y. Xia, M. Ng, Y. C. Teh, L. Tan, M. Evrard, J. L. Li, H. T. Tran, Y. Tan, *et al.*, Combinatorial single-cell analyses of granulocyte-monocyte progenitor heterogeneity reveals an early uni-potent neutrophil progenitor, *Immunity* **53**, 303 (2020).
- [30] C. H. Waddington, *The strategy of the genes* (Routledge, 2014).
- [31] R. A. Nimmo, G. E. May, and T. Enver, Primed and ready: understanding lineage commitment through single cell analysis, *Trends in cell biology* **25**, 459 (2015).
- [32] A. G. Erickson, P. Kameneva, and I. Adameyko, The transcriptional portraits of the neural crest at the individual cell level, in *Seminars in cell & developmental biology*, Vol. 138 (Elsevier, 2023) pp. 68–80.

Appendix for *Hierarchical Control of State Transitions in Dense Associative Memories*

Contents

A	Coarse-graining	2
A.1	Coarse-graining transformation for patterns of identical magnitude	2
A.2	Invariance of dynamics to transformation for identical memory patterns	3
A.3	Coarse-graining for general patterns of identical magnitude	3
A.3.1	Similarity of the coarse-grained energy function in the two-pattern case	3
A.3.2	Coarse-graining for subsets of many patterns	4
A.4	Coarse-graining transformation for patterns of arbitrary magnitude	5
B	Dimensionality reduction of the dynamics	6
C	Dynamics in the vicinity of the coarse-grained pattern	7
D	w-Modulation of the energy function and basins of attraction	8
D.1	Estimation of the basins of attractions	9
D.1.1	Theoretical considerations	9
D.1.2	Eigenvalues of the Hessian	9
D.1.3	Calculation of the estimated separatrix	13
D.2	Separatrix between two patterns	14
D.2.1	Effect of a far away pattern on the separatrix	15
D.3	Control of progenitor basins by modulation of \mathbf{w}	15
E	Local instability and the calculation of β_{crit} for equal-angle patterns	16
F	Model for cell identity regulation	19
F.1	General model for gene regulatory network based on enhancer selection	19
F.2	Symmetric dynamics derived from autoregulatory dynamics	20
F.3	Simulation of annealing in blood production	20

arXiv:2412.11336v1 [q-bio.CB] 15 Dec 2024

A Coarse-graining

1 Coarse-graining transformation for patterns of identical magnitude

In this section, we present the coarse graining transformation for patterns of identical magnitude and inspect its mathematical properties. Suppose we have N nodes (TFs in the gene regulatory network) and K memory patterns. The dynamics of the system are given by:

$$\dot{\mathbf{x}} = g(\mathbf{x}, \beta, \mathbf{Q}, \Xi, \mathbf{w}) = \mathbf{Q}^T \text{softmax}(\beta \Xi \mathbf{x} + \mathbf{w}) - \mathbf{x} \quad (1)$$

We consider a subset of indices $\mathcal{L} \subseteq \{1 \dots K\}$ and define our coarse-graining transformation for patterns of identical magnitude by $\mathbf{Q} \xrightarrow{\mathcal{L}} \mathbf{Q}'$, $\Xi \xrightarrow{\mathcal{L}} \Xi'$, $\mathbf{w} \xrightarrow{\mathcal{L}} \mathbf{w}'$, where:

$$\mathbf{Q}' = \mathbf{Q}_{i \notin \mathcal{L}} \cup \{Q_{\mathcal{L}}^*\}, \quad \Xi' = \Xi_{i \notin \mathcal{L}} \cup \{\Xi_{\mathcal{L}}^*\}, \quad \mathbf{w}' = \mathbf{w}_{i \notin \mathcal{L}} \cup \{w_{\mathcal{L}}^*\} \quad (2)$$

with:

$$\begin{aligned} Q_{\mathcal{L}}^* &= \frac{\sum_{i \in \mathcal{L}} Q_i e^{w_i}}{\sum_{i \in \mathcal{L}} e^{w_i}} = \text{softmax}(\mathbf{w}_{i \in \mathcal{L}}) Q_{i \in \mathcal{L}} \\ \Xi_{\mathcal{L}}^* &= \frac{\sum_{i \in \mathcal{L}} \Xi_i e^{w_i}}{\sum_{i \in \mathcal{L}} e^{w_i}} = \text{softmax}(\mathbf{w}_{i \in \mathcal{L}}) \Xi_{i \in \mathcal{L}} \\ w_{\mathcal{L}}^* &= \log \sum_{k \in \mathcal{L}} e^{w_k} \end{aligned} \quad (3)$$

This transforms the dimension of the matrices from $N \times K$ to $N \times K'$ with $K' = K - |\mathcal{L}| + 1$. We denote the transformed dynamics as $g_{\mathcal{L}}(\mathbf{x}, \beta, \mathbf{Q}, \Xi, \mathbf{w})$.

We will begin by showing that the order in which we apply the coarse-graining transformation in Eq. 3 does not matter, i.e. our transformation is in essence commutative. More precisely, consider two subsets of indices $\mathcal{L}_1, \mathcal{L}_2 \subseteq \{1, \dots, K\}$, such that $\mathcal{L}_1 \cap \mathcal{L}_2 = \emptyset$ and let $\mathcal{L} = \mathcal{L}_1 \cup \mathcal{L}_2$. We let $L_{1,Q}$ be the transformation corresponding to the transformation in Eq. 3 above with indices given by \mathcal{L}_1 acting on the \mathbf{Q} matrices, and similarly for Ξ and \mathbf{w} . We define $L_{1,Q} \odot L_{2,Q}$ as the transformation that reduces all rows given by indices in \mathcal{L}_2 to one row (as above) and then reducing all the indices in \mathcal{L}_1 (with the labelling corresponding to the original labelling) to one row.

Proposition A.1. *When $\mathcal{L}_1 \cap \mathcal{L}_2 = \emptyset$, we have $L_{1,Q} \odot L_{2,Q} = L_{2,Q} \odot L_{1,Q}$ and similarly for transformations acting on Ξ and \mathbf{w} .*

Proof. Note that as $\mathcal{L}_1 \cap \mathcal{L}_2 = \emptyset$, $L_{1,Q} \odot L_{2,Q}(\mathbf{Q}) = L_{1,Q}(\mathbf{Q}_{i \notin \mathcal{L}_2} \cup \{Q_{\mathcal{L}_2}^*\}) = \mathbf{Q}_{i \notin \mathcal{L}_1} \cup \mathbf{Q}_{i \notin \mathcal{L}_2} \cup \{Q_{\mathcal{L}_1}^*\} \cup \{Q_{\mathcal{L}_2}^*\}$ and so

$$L_{1,Q} \odot L_{2,Q} = L_{2,Q} \odot L_{1,Q}.$$

Exactly the same arguments work for $L_{1,\mathbf{w}}$ and $L_{1,\Xi}$. □

Now suppose as above that $\mathcal{L}_1, \mathcal{L}_2 \subseteq \{1, \dots, K\}$, such that $\mathcal{L}_1 \cap \mathcal{L}_2 = \emptyset$ and let $\mathcal{L} = \mathcal{L}_1 \cup \mathcal{L}_2$. And let L_1, L_2, L be the corresponding maps (acting on the same variables, i.e. either \mathbf{Q}, \mathbf{w} or Ξ), further define the map L^* as the map associated with the transformation given by the indices $\mathcal{L}^* = \{1^*, 2^*\}$, where $1^*, 2^*$ are the indices to which \mathcal{L}_1 and \mathcal{L}_2 are mapped respectively. Then we have the following:

Proposition A.2. *Suppose $\mathcal{L}_1, \mathcal{L}_2 \subseteq \{1, \dots, K\}$ such that $\mathcal{L}_1 \cap \mathcal{L}_2 = \emptyset$ and let $\mathcal{L} = \mathcal{L}_1 \cup \mathcal{L}_2$. Then $L = L^* \odot L_1 \odot L_2$ for $\mathbf{Q}, \Xi, \mathbf{w}$.*

Proof. Consider \mathbf{Q} , then from the previous proposition we know that $L_{1,Q} \odot L_{2,Q}(\mathbf{Q}) = \mathbf{Q}_{i \notin \mathcal{L}_1} \cup \mathbf{Q}_{i \notin \mathcal{L}_2} \cup \{Q_{\mathcal{L}_1}^*\} \cup \{Q_{\mathcal{L}_2}^*\}$. Therefore we have that

$$L = L^* \odot L_1 \odot L_2(\mathbf{Q}) = \mathbf{Q}_{i \notin \mathcal{L}} \cup \{Q_{\mathcal{L}_{\{1,2\}}}^{**}\},$$

where $Q_{\mathcal{L}_{\{1,2\}}}^{**}$ is given by

$$Q_{\mathcal{L}_{\{1,2\}}}^{**} = \frac{Q_1^* e^{w_1^*} + Q_2^* e^{w_2^*}}{e^{w_1^*} + e^{w_2^*}}.$$

As such to prove our claim we need to show that

$$\frac{Q_1^* e^{w_1^*} + Q_2^* e^{w_2^*}}{e^{w_1^*} + e^{w_2^*}} = \frac{\sum_{i \in \mathcal{L}} Q_i e^{w_i}}{\sum_{i \in \mathcal{L}} e^{w_i}}.$$

Now note that $\exp(w_1^*) = \sum_{j \in \mathcal{L}_1} \exp(w_j)$. Thus

$$Q_{\mathcal{L}_1}^* e^{w_1^*} = \sum_{i \in \mathcal{L}_1} Q_i,$$

and as such we precisely have that

$$\frac{Q_1^* e^{w_1^*} + Q_2^* e^{w_2^*}}{e^{w_1^*} + e^{w_2^*}} = \frac{\sum_{i \in \mathcal{L}} Q_i e^{w_i}}{\sum_{i \in \mathcal{L}} e^{w_i}},$$

which concludes our proof for \mathbf{Q} . Similar arguments show the equivalence for Ξ, \mathbf{w} . \square

As such we see that our transformations are commutative and the sequential application of transformations corresponds to the application of one transformation on the entire set of indices.

2 Invariance of dynamics to transformation for identical memory patterns

We will show that the application of the transformation in Eq. 3 on identical patterns (identical rows of Ξ) leaves the dynamics invariant. This has been previously demonstrated in Karin [1] and is included here for completeness.

Proposition A.3. *Consider a subset \mathcal{L} such that for each $r, s \in \mathcal{L}$ we have that $\Xi_r = \Xi_s$. Then $g(\mathbf{x}, \beta, \mathbf{Q}, \Xi, \mathbf{w}) = g_{\mathcal{L}}(\mathbf{x}, \beta, \mathbf{Q}, \Xi, \mathbf{w})$.*

Proof. Consider the original dynamics for x_j :

$$\begin{aligned} \dot{x}_j &= \sum_{i=1}^K q_{i,j} \frac{e^{w_i + \beta \sum_l \xi_{i,l} x_l}}{\sum_k e^{w_k + \beta \sum_l \xi_{k,l} x_l}} - x_j = \\ &= \sum_{i \in \mathcal{L}} \frac{q_{i,j} e^{w_i + \beta \sum_l \xi_{i,l} x_l}}{\sum_{k \in \mathcal{L}} e^{w_k + \beta \sum_l \xi_{k,l} x_l} + \sum_{k \notin \mathcal{L}} e^{w_k + \beta \sum_l \xi_{k,l} x_l}} + \sum_{i \notin \mathcal{L}} \frac{q_{i,j} e^{w_i + \beta \sum_l \xi_{i,l} x_l}}{\sum_{k \in \mathcal{L}} e^{w_k + \beta \sum_l \xi_{k,l} x_l} + \sum_{k \notin \mathcal{L}} e^{w_k + \beta \sum_l \xi_{k,l} x_l}} - x_j \end{aligned}$$

Now, under the transformation, and noting that for $k \in \mathcal{L}$ we have that $\Xi_k = \Xi_{\mathcal{L}}^*$, we have:

$$\sum_{k \in \mathcal{L}} e^{w_k + \beta \sum_l \xi_{k,l} x_l} = \sum_{k \in \mathcal{L}} e^{w_k + \beta \Xi_{\mathcal{L}}^* \cdot \mathbf{x}} = e^{w_{\mathcal{L}}^* + \beta \Xi_{\mathcal{L}}^* \cdot \mathbf{x}}$$

And:

$$\sum_{k \in \mathcal{L}} q_{k,j} e^{w_k + \beta \sum_l \xi_{k,l} x_l} = e^{\beta \Xi_{\mathcal{L}}^* \cdot \mathbf{x}} \sum_{k \in \mathcal{L}} q_{k,j} e^{w_k} = (Q_{\mathcal{L}}^*)_j e^{w_{\mathcal{L}}^* + \beta \Xi_{\mathcal{L}}^* \cdot \mathbf{x}}$$

And thus the transformed dynamics are given by:

$$\begin{aligned} \dot{x}_j &= \frac{(Q_{\mathcal{L}}^*)_j e^{w_{\mathcal{L}}^* + \beta \Xi_{\mathcal{L}}^* \cdot \mathbf{x}}}{e^{w_{\mathcal{L}}^* + \beta \Xi_{\mathcal{L}}^* \cdot \mathbf{x}} + \sum_{k \notin \mathcal{L}} e^{w_k + \beta \sum_l \xi_{k,l} x_l}} + \sum_{i \notin \mathcal{L}} q_{i,j} \frac{e^{w_i + \beta \sum_l \xi_{i,l} x_l}}{e^{w_{\mathcal{L}}^* + \beta \Xi_{\mathcal{L}}^* \cdot \mathbf{x}} + \sum_{k \notin \mathcal{L}} e^{w_k + \beta \sum_l \xi_{k,l} x_l}} - x_j \\ &= \sum_{i \notin \mathcal{L} \text{ or } i=*} q_{i,j} \frac{e^{w_i + \beta \sum_l \xi_{i,l} x_l}}{\sum_k e^{w_k + \beta \sum_l \xi_{k,l} x_l}} - x_j \end{aligned}$$

And thus the dynamics are invariant under the transformation. \square

3 Coarse-graining for general patterns of identical magnitude

A.3.1 Similarity of the coarse-grained energy function in the two-pattern case

Throughout this section we suppose that the patterns in question have equal magnitude, which without loss of generality we set to unity. Our analysis will focus on the symmetric case, namely when $\mathbf{Q} = \Xi$ so that we have an energy functional:

$$V(\mathbf{x}, \beta, \Xi, \mathbf{w}) = -\beta^{-1} \log(Z) + \|\mathbf{x}\|^2/2 \quad (4)$$

with $Z = \sum_i e^{\beta \Xi_i \cdot \mathbf{x} + w_i}$. Notice that the values that $V(\mathbf{x})$ takes are, in general, of order unity. The main idea is that now, while the transformed dynamics are not identical to the original dynamics, they are similar to the original dynamics up to a perturbative term of order $\beta \mu^2$ with μ being the angle between the patterns; and thus for a small enough β the dynamics will be effectively identical. To see this, consider a coarse-graining transformation on the indices \mathcal{L} and let $V_{\mathcal{L}}(\mathbf{x})$ be the coarse-grained energy functional. Then we have that

$$V_{\mathcal{L}}(\mathbf{x}) - V(\mathbf{x}) = \frac{1}{\beta} \left(\log \left(\sum_{i=1}^K e^{(w_i + \beta \Xi_i \cdot \mathbf{x})} \right) - \log \left(e^{(w_{\mathcal{L}}^* + \beta \Xi_{\mathcal{L}}^* \cdot \mathbf{x})} + \sum_{i \notin \mathcal{L}} e^{(w_i + \beta \Xi_i \cdot \mathbf{x})} \right) \right).$$

And thus if we let $R = \sum_{i \notin \mathcal{L}} e^{w_i + \beta \Xi_i \cdot \mathbf{x}}$, we have

$$V_{\mathcal{L}}(\mathbf{x}) - V(\mathbf{x}) = \frac{1}{\beta} \left(\log(R + \sum_{i \in \mathcal{L}} e^{(w_i + \beta \Xi_i \cdot \mathbf{x})}) - \log(R + e^{(w_{\mathcal{L}}^* + \beta \Xi_{\mathcal{L}}^* \cdot \mathbf{x})}) \right).$$

If \mathcal{L} is just two indices, $\mathcal{L} = \{r, s\}$, the above reads

$$V_{\mathcal{L}}(\mathbf{x}) - V(\mathbf{x}) = \frac{1}{\beta} \left(\log(R + [e^{(w_r + \beta \Xi_r \cdot \mathbf{x})} + e^{(w_s + \beta \Xi_s \cdot \mathbf{x})}]) - \log \left(R + [e^{w_s} + e^{w_r}] e^{\beta \frac{e^{w_s} \Xi_s \cdot \mathbf{x} + e^{w_r} \Xi_r \cdot \mathbf{x}}{e^{w_s} + e^{w_r}}} \right) \right).$$

Let $\theta - \phi, \theta + \phi, \mu_{r,s}$ denote $\angle(\Xi_r, \mathbf{x}), \angle(\Xi_s, \mathbf{x}), \angle(\Xi_r, \Xi_s)$, noting that from the triangle inequality of angles we have that $\phi \leq \mu_{r,s}/2$. Recall that we assume $\|\Xi_r\| = \|\Xi_s\| = 1$. Then we have that $\beta(V_{\mathcal{L}}(\mathbf{x}) - V(\mathbf{x}))$ is equal to

$$\log(R + [e^{(w_r + \beta \|\mathbf{x}\| \cos(\theta - \phi))} + e^{(w_s + \beta \|\mathbf{x}\| \cos(\theta + \phi))}]) - \log(R + [e^{w_s} + e^{w_r}] e^{\beta \|\mathbf{x}\| \frac{e^{w_s} \cos(\theta - \phi) + e^{w_r} \cos(\theta + \phi)}{e^{w_s} + e^{w_r}}}).$$

Expanding around a small angle $\phi \ll 1$, we get that

$$V_{\mathcal{L}}(\mathbf{x}) - V(\mathbf{x}) = \frac{2\beta \|\mathbf{x}\|^2 \sin^2(\theta) \phi^2 e^{\beta \|\mathbf{x}\| \cos(\theta) + w_r + w_s}}{(e^{w_r} + e^{w_s})(e^{\beta \|\mathbf{x}\| \cos(\theta)}(e^{w_r} + e^{w_s}) + R)} + \mathcal{O}(\phi^3).$$

By letting

$$\nu = \frac{2e^{\beta \|\mathbf{x}\| \cos(\theta) + w_r + w_s}}{(e^{w_r} + e^{w_s})(e^{\beta \|\mathbf{x}\| \cos(\theta)}(e^{w_r} + e^{w_s}) + R)},$$

we can find an upper bound in the following way.

$$\nu \leq \frac{2e^{w_r + w_s}}{(e^{w_r} + e^{w_s})^2} \leq \frac{1}{2},$$

with the final inequality following from the AM-GM inequality. From this we in particular have that

$$V_{\mathcal{L}}(\mathbf{x}) - V(\mathbf{x}) = \beta \nu \|\mathbf{x}\|^2 \sin^2(\theta) \phi^2 + \mathcal{O}(\phi^3) \leq \frac{1}{8} \beta \mu^2$$

where in the last inequality we also used $\|\mathbf{x}\| \leq 1$.

A.3.2 Coarse-graining for subsets of many patterns

Our previous results can be generalized in a straightforward manner to subsets of many patterns. Consider a set of unit vector patterns Ξ_1, \dots, Ξ_n and a vector \mathbf{x} such that the angle between \mathbf{x} and pattern i is denoted $\angle(\Xi_i, \mathbf{x}) = \theta + k_i \phi$ (we may set θ as the minimal angle between \mathbf{x} and any of the patterns). We denote the set of indices of patterns we are coarse-graining by \mathcal{L} , and we set $\angle(\Xi_i, \Xi_j) = \mu_{ij}$ (with $\mu_{\mathcal{L}}$ as the maximal angle between any two patterns in \mathcal{L}). We have, from the triangle inequality of angles:

$$\mu_{ij} + \theta + k_i \phi \geq \theta + k_j \phi$$

And thus:

$$\mu_{ij} \geq (k_j - k_i) \phi$$

Consider the energy difference:

$$\begin{aligned} V_{\mathcal{L}}(\mathbf{x}) - V(\mathbf{x}) &= \frac{1}{\beta} \left(\log(R + \sum_{i \in \mathcal{L}} e^{w_i + \beta \Xi_i \cdot \mathbf{x}}) - \log \left(R + e^{w_{\mathcal{L}}^* + \beta \Xi_{\mathcal{L}}^* \cdot \mathbf{x}} \right) \right) \\ &= \frac{1}{\beta} \left(\log(R + \sum_{i \in \mathcal{L}} e^{w_i + \beta \Xi_i \cdot \mathbf{x}}) - \log \left(R + \sum_{i \in \mathcal{L}} e^{w_i} e^{\beta \frac{\sum_{i \in \mathcal{L}} e^{w_i} \Xi_i \cdot \mathbf{x}}{\sum_{i \in \mathcal{L}} e^{w_i}}} \right) \right) \\ &= \frac{1}{\beta} \left(\log(R + \sum_{i \in \mathcal{L}} e^{w_i + \beta \|\mathbf{x}\| \cos(\theta + k_i \phi)}) - \log \left(R + \sum_{i \in \mathcal{L}} e^{w_i} e^{\beta \frac{\sum_{i \in \mathcal{L}} e^{w_i} \beta \|\mathbf{x}\| \cos(\theta + k_i \phi)}{\sum_{i \in \mathcal{L}} e^{w_i}}} \right) \right) \end{aligned}$$

We can expand over ϕ to a second order:

$$\begin{aligned}
|V_{\mathcal{L}}(\mathbf{x}) - V(\mathbf{x})| &\approx \frac{\sum_{i,j \in \mathcal{L}, i < j} (k_i - k_j)^2 e^{w_i + w_j}}{\frac{2 \sum_{i \in \mathcal{L}} e^{w_i}}{e^{\beta \cos(\theta)}} R + 2 (\sum_{i \in \mathcal{L}} e^{w_i})^2} \beta \|\mathbf{x}\|^2 \phi^2 \sin^2(\theta) \\
&\leq \frac{\sum_{i,j \in \mathcal{L}, i < j} (k_i - k_j)^2 e^{w_i + w_j}}{(\sum_{i \in \mathcal{L}} e^{w_i})^2} \frac{\beta \|\mathbf{x}\|^2 \phi^2 \sin^2(\theta)}{2} \\
&\leq \frac{\sum_{i,j \in \mathcal{L}, i < j} e^{w_i + w_j}}{(\sum_{i \in \mathcal{L}} e^{w_i})^2} \frac{\beta \|\mathbf{x}\|^2 \mu_{\mathcal{L}}^2 \sin^2(\theta)}{2} \\
&= \frac{\sum_{i,j \in \mathcal{L}, i < j} e^{w_i + w_j}}{2 \sum_{i,j \in \mathcal{L}, i < j} e^{w_i + w_j} + \sum_{i \in \mathcal{L}} e^{2w_i}} \frac{\beta \|\mathbf{x}\|^2 \mu_{\mathcal{L}}^2 \sin^2(\theta)}{2} \\
&\leq \frac{\sin^2(\theta)}{4} \beta \mu_{\mathcal{L}}^2 \leq \frac{1}{4} \beta \mu_{\mathcal{L}}^2
\end{aligned}$$

The coarse grained dynamics are thus similar to the fine-grained dynamics when $\beta \ll 1/\mu_{\mathcal{L}}^2$.

4 Coarse-graining transformation for patterns of arbitrary magnitude

We will now generalize the coarse-graining transformation to be valid for patterns of any magnitude. The idea behind the generalized transformation is identical to the previous sections - we will look for a transformation for which the transformed dynamics are identical to the original dynamics up to a factor of magnitude $\beta \mu_{\mathcal{L}}^2$. For a subset of indices $\mathcal{L} \subseteq \{1 \dots K\}$ corresponding to patterns of magnitudes $u_i, i \in \mathcal{L}$, we define our coarse-graining transformation by $\mathbf{Q} \xrightarrow{\mathcal{L}} \mathbf{Q}', \Xi \xrightarrow{\mathcal{L}} \Xi', \mathbf{w} \xrightarrow{\mathcal{L}} \mathbf{w}'$, where:

$$\mathbf{Q}' = \mathbf{Q}_{i \notin \mathcal{L}} \cup \{Q_{\mathcal{L}}^*\}, \quad \Xi' = \Xi_{i \notin \mathcal{L}} \cup \{\Xi_{\mathcal{L}}^*\}, \quad \mathbf{w}' = \mathbf{w}_{i \notin \mathcal{L}} \cup \{w_{\mathcal{L}}^*\}$$

with:

$$\begin{aligned}
Q_{\mathcal{L}}^* &= \frac{\sum_{i \in \mathcal{L}} Q_i e^{w_i + \beta u_i}}{\sum_{i \in \mathcal{L}} e^{w_i + \beta u_i}} = \text{softmax}(\mathbf{w}_{i \in \mathcal{L}} + \beta \mathbf{u}_{i \in \mathcal{L}}) Q_{i \in \mathcal{L}} \\
\Xi_{\mathcal{L}}^* &= \frac{\sum_{i \in \mathcal{L}} \Xi_i e^{w_i + \beta u_i}}{\sum_{i \in \mathcal{L}} e^{w_i + \beta u_i}} = \text{softmax}(\mathbf{w}_{i \in \mathcal{L}} + \beta \mathbf{u}_{i \in \mathcal{L}}) \Xi_{i \in \mathcal{L}} \\
w_{\mathcal{L}}^* &= -\frac{\sum_{i \in \mathcal{L}} u_i e^{w_i + u_i \beta}}{\sum_{i \in \mathcal{L}} e^{w_i + u_i \beta}} \beta + \log \sum_{k \in \mathcal{L}} e^{w_k + u_k \beta} = -\text{softmax}(\mathbf{w}_{i \in \mathcal{L}} + \beta \mathbf{u}_{i \in \mathcal{L}}) \cdot \beta \mathbf{u} + \log \sum_{k \in \mathcal{L}} e^{w_k + u_k \beta}
\end{aligned} \tag{5}$$

While the transformation appears similar to the equal magnitude case, a key difference is the β -dependence, where at large β the largest pattern dominates the transformation. For an example of the application of the transformation, see Fig. 1.

Similar to the equal-magnitude case, this transformation is self-similar. It also maintains symmetry - if $Q_i = \Xi_i$ for all $i \in \mathcal{L}$ then $Q_{\mathcal{L}}^* = \Xi_{\mathcal{L}}^*$. The transformation coarse-grains the energy function in a similar manner to the equal-magnitude case, namely by:

$$V_{\mathcal{L}}(\mathbf{x}, \beta, \Xi, \mathbf{w}) = V(\mathbf{x}, \beta, \Xi', \mathbf{w}') + \mathcal{O}(\beta \mu_{\mathcal{L}}^2)$$

where here the $\mathcal{O}(\beta \mu_{\mathcal{L}}^2)$ involves a more complex dependence on the magnitudes.

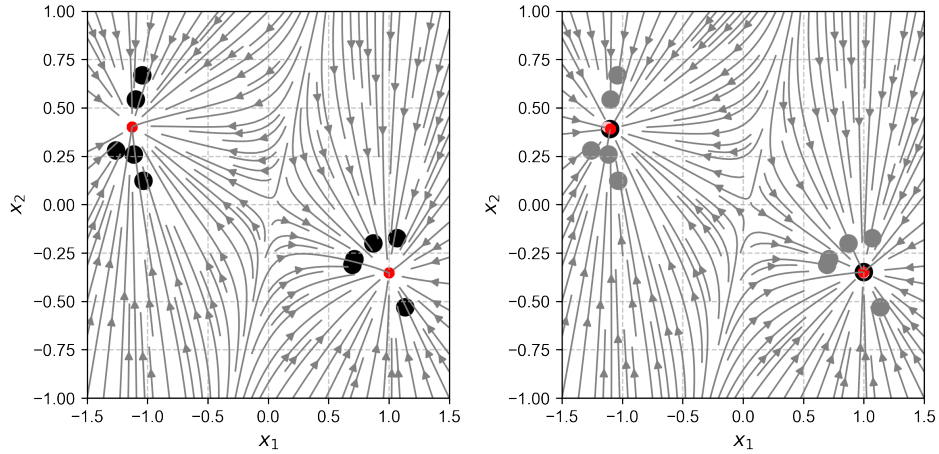


Figure 1: Example of application of transformation for patterns of arbitrary magnitude.

Left: Dynamics at $\beta = 3$ for two clustered sets of patterns (black dots correspond to patterns, red dots correspond to stable fixed points). Right: Coarse-grained dynamics with the transformation 5 applied to pattern clusters. Black dots correspond to coarse-grained patterns, red dots correspond to stable fixed points, gray dots correspond to fine-grained patterns and pink dots to stable fixed points of the original dynamics.

B Dimensionality reduction of the dynamics

In this section we will demonstrate that it is possible to capture the dynamics of a system in a reduced form based on dimensionality reduction and rotation. Consider the dynamics given by Eq. 1, where the dimensions of \mathbf{Q}, Ξ are $K \times N$. We can see that \mathbf{x} is confined to the convex hull whose vertices are the rows of \mathbf{Q} (since softmax produces a probability vector). This convex hull is a subspace of dimension at most $K - 1$. In addition, the dynamics of Eq. 1 are invariant to orthogonal transformations. This is the subject of the following proposition:

Proposition B.1. *Let $\mathbf{M} \in \mathbb{R}^{N \times N}$ be an orthogonal matrix. Then if \mathbf{x} satisfies Eq. 1, with \mathbf{Q}, Ξ , then $\mathbf{y} = \mathbf{M}\mathbf{x}$, satisfies Eq. 1 with $\tilde{\mathbf{Q}} = \mathbf{Q}\mathbf{M}^T, \tilde{\Xi} = \Xi\mathbf{M}^T$.*

Proof. We have that $\dot{\mathbf{y}} = \mathbf{M}\dot{\mathbf{x}}$ and so from Eq. 1

$$\dot{\mathbf{y}} = \mathbf{M}\mathbf{Q}^T \text{softmax}(\beta\Xi\mathbf{x} + \mathbf{w}) - \mathbf{y}$$

By the fact that \mathbf{M} is an orthogonal matrix we have $\mathbf{M}^T\mathbf{M} = \mathbf{I}$ and so

$$\dot{\mathbf{y}} = \tilde{\mathbf{Q}}^T \text{softmax}(\beta\tilde{\Xi}\mathbf{y} + \mathbf{w}) - \mathbf{y}.$$

□

Now we will examine how the invariance of the dynamics of Eq. 1 to orthogonal transformations, can lead to the decoupling of the dynamics of some of the components, and how in the symmetric case, where we have a potential given by Eq. 4, it leads to a dimensional reduction. Consider the case where $N > K$, and let \mathbf{A} be a $K \times N$ real matrix. We may apply the singular value decomposition to get $\mathbf{A} = \mathbf{U}\mathbf{S}\mathbf{V}^T$, where \mathbf{U} is a $K \times K$ orthogonal matrix, \mathbf{V} is a $N \times N$ orthogonal matrix, and \mathbf{S} is a $K \times N$ matrix, with the diagonal entries corresponding to the singular values of \mathbf{A} , and the rest of the entries being zeros. Crucially note that *the number of non-zero entries of \mathbf{S} is equal to the rank of \mathbf{A}* . Multiplying by \mathbf{V} , and calling this quantity, $\tilde{\mathbf{A}}$, we get that

$$\tilde{\mathbf{A}} := \mathbf{A}\mathbf{V} = \mathbf{U}\mathbf{S}.$$

Now consider the form $\tilde{\mathbf{A}}$ takes. By choosing appropriate \mathbf{V}, \mathbf{U} in the decomposition, we may always ensure that the diagonal entries of \mathbf{S} appear in descending order, i.e. $d_1 \geq d_2 \geq \dots \geq d_K \geq 0$ (note that singular values will always be non-negative). I.e. \mathbf{S} has the following block form

$$\mathbf{S} = \left(\begin{array}{cccc|c} d_1 & 0 & 0 & \dots & 0 \\ 0 & d_2 & 0 & \dots & 0 \\ \vdots & \vdots & \vdots & \ddots & \vdots \\ 0 & \dots & 0 & d_{K-1} & 0 \\ 0 & \dots & \dots & 0 & d_K \end{array} \right) \mathbf{0}$$

So if we look at the ij^{th} component of $\tilde{\mathbf{A}}$, we get

$$\tilde{a}_{ij} = \sum_{r=1}^K u_{ir} s_{rj} = \begin{cases} \sum_{r=1}^K u_{ir} \delta_{rj} d_j & \text{if } j \leq K \\ 0 & \text{otherwise} \end{cases}.$$

And thus

$$\tilde{a}_{ij} = \begin{cases} u_{ij} d_j & \text{if } j \leq K \\ 0 & \text{otherwise} \end{cases}.$$

Thus for any column m , of $\tilde{\mathbf{A}}$ such that $N \geq m > K$, all the entries of that column will be 0.

Therefore returning to the dynamics of Eq. 1, and considering the singular value decomposition for $\mathbf{A} = \mathbf{Q}$, with the transformation of proposition B.1 given by $\mathbf{M}^T = \mathbf{V}$, we get that the dynamics of our equation will be given by

$$\dot{\mathbf{y}} = \tilde{\mathbf{Q}}^T \text{softmax}(\beta \tilde{\Xi} \mathbf{y} + \mathbf{w}) - \mathbf{y},$$

and from our particular choice of the transformation we know that for $K < j \leq N$, we have

$$\dot{y}_j = -y_j, \tag{6}$$

since

$$\sum_{k=1}^N q_{kj} [\text{softmax}(\beta \tilde{\Xi} \mathbf{y} - \mathbf{w})]_k = 0.$$

From this we deduce that our system decouples, with the dynamics of y_j for $j \geq K$ being completely determined¹. Now this means that in the general case of the dynamics being given by Eq. 1, provided our dynamics start at $\mathbf{0}$, we can reduce the dynamics of our system from N to K dimensions.

However, in the symmetric case when $\mathbf{Q} = \Xi$, i.e. our system is given by a potential function as in Eq. 4, we do get a full decoupling of the system, as now

$$\sum_{r=1}^N \tilde{\xi}_{ir} y_r = \sum_{r=1}^K \tilde{\xi}_{ir} y_r,$$

as $\mathbf{Q} = \Xi$ and so $\tilde{\xi}_{ir} = 0$, for $r > K$. And as such, with our orthogonal transformation, we reduce the dimension of the system from N to K .

C Dynamics in the vicinity of the coarse-grained pattern

We want to understand the local dynamics of the system. One would expect that when you are close to a coarse-grained pattern Ξ^* , the patterns that contribute to the dynamics, are precisely the ones that form the coarse-grained pattern. This is indeed the case as we will see below, for a parameter regime, which we will derive in this section.

As before suppose all patterns have a magnitude of unity and suppose we have two isolated patterns in our system, Ξ_r, Ξ_s , i.e. we have that for $l \neq r, s$, $\mu_{l,s} \ll \mu_{l,r}$ and $\mu_{r,s} \ll \mu_{l,s}$, where μ_{ij} is the angle between patterns i and j . Let us also define μ_m to be the value, such that $\mu_m = \min_{l \neq r,s} \{\mu_{l,s}, \mu_{l,r}\}$, i.e. μ_m is the smallest angle of separation between the isolated patterns and the rest of the patterns. We are interested in the dynamics in the vicinity of the progenitor pattern of the two isolated patterns, that is, we consider \mathbf{x} such that

$$\mathbf{x} = \Xi^* + \mathbf{y},$$

where \mathbf{y} is some perturbation away from the coarse-grained pattern. The only restriction we place on \mathbf{y} is that it must lie in the region "between" the two patterns Ξ_r, Ξ_s , i.e. for any non-isolated pattern Ξ_i , we must have $\angle(\Xi_i, \mathbf{y}) \geq \mu_m$, while for the isolated patterns we have $\angle(\mathbf{y}, \Xi_r) \leq \angle(\Xi_r, \Xi_s)$ and $\angle(\mathbf{y}, \Xi_s) \leq \angle(\Xi_r, \Xi_s)$. Then our dynamical system can be written as

$$\dot{\mathbf{y}} = \mathbf{Q}^T \text{softmax}(\beta \Xi(\Xi^* + \mathbf{y}) + \mathbf{w}) - \mathbf{y} - \Xi^*.$$

Writing out the i^{th} component of the soft-max, we have

$$[\text{softmax}(\beta \Xi(\Xi^* + \mathbf{y}) + \mathbf{w})]_i = \frac{1}{Z} e^{(\beta(\Xi_i \cdot \Xi^* + \Xi_i \cdot \mathbf{y}) + w_i)} \tag{7}$$

$$= \frac{1}{Z} e^{\beta \left(\frac{\cos(\mu_{i,r}) e^{w_r} + \cos(\mu_{i,s}) e^{w_s}}{e^{w_r} + e^{w_s}} + \Xi_i \cdot \mathbf{y} \right) + w_i} \tag{8}$$

¹In fact since the number of non-zero singular values is the same as the rank of the matrix, if \mathbf{Q} has a smaller rank, $R < K$ then y_j will decouple for all $j > R$

Now consider in particular a pattern, Ξ_i , which is not one of the two isolated ones, so that $i \neq r, s$. Now $\mu_m \leq \mu_{r,s}$ and as such $\cos(\mu_m) \geq \cos(\mu_{r,s})$. Therefore we can bound the i^{th} soft-max component, as follows

$$[\text{softmax}(\beta\Xi(\Xi^* + \mathbf{y}) + \mathbf{w})]_i \leq \frac{1}{Z} e^{\beta(\cos(\mu_m) + \Xi_i \cdot \mathbf{y}) + w_i}$$

Now recall we consider \mathbf{y} , such that the angle between \mathbf{y} satisfies $\angle(\Xi_i, \mathbf{y}) \geq \mu_m$, and therefore $\cos(\angle(\Xi_i, \mathbf{y})) \leq \cos(\mu_m)$. From this we get the further bound

$$[\text{softmax}(\beta\Xi(\Xi^* + \mathbf{y}) + \mathbf{w})]_i \leq \frac{1}{Z} e^{\beta \cos(\mu_m)(1 + \|\mathbf{y}\|) + w_i} \quad (9)$$

If we consider (without loss of generality) the r^{th} component of the soft-max (i.e. one corresponding to one of the isolated patterns), we get from Eq. 8 that

$$[\text{softmax}(\beta\Xi(\Xi^* + \mathbf{y}))]_r = \frac{1}{Z} e^{\beta \left(\frac{e^{w_r} + \cos(\mu_{r,s})e^{w_s}}{e^{w_r} + e^{w_s}} + \Xi_r \cdot \mathbf{y} \right) + w_i}$$

Recall that we chose \mathbf{y} above, such that we have $\angle(\mathbf{y}, \Xi_r) \leq \angle(\Xi_r, \Xi_s)$ and as such $\cos(\angle(\Xi_r, \Xi_s)) \geq \cos(\mu_{r,s})$. By further setting $p = e^{w_r} / (e^{w_r} + e^{w_s})$, we get

$$[\text{softmax}(\beta\Xi(\Xi^* + \mathbf{y}))]_r \geq \frac{1}{Z} e^{\beta(p + (1-p)\cos(\mu_{r,s}) + \|\mathbf{y}\|\cos(\mu_{r,s})) + w_i} \quad (10)$$

With this preliminary calculation, we now look at the ratio of the soft-max components of a non-isolated pattern, compared to an isolated pattern. Let's call this ratio \mathcal{S} , i.e.

$$\mathcal{S} = \frac{[\text{softmax}(\beta\Xi(\Xi^* + \mathbf{y}) + \mathbf{w})]_i}{[\text{softmax}(\beta\Xi(\Xi^* + \mathbf{y}) + \mathbf{w})]_r}$$

The reason we are looking at this ratio is as follows. If $\mathcal{S} \ll 1$, then that would mean that the isolated pattern dominates the non-isolated one, and as such we are safe to ignore the contribution of the non-isolated patterns. While if $\mathcal{S} \ll 1$, then the non-isolated patterns do contribute to an extent, which we cannot ignore. With this we look at \mathcal{S} , and by combining Eq. 9 and Eq. 10 we get

$$\mathcal{S} \leq \frac{e^{\beta \cos(\mu_m)(1 + \|\mathbf{y}\|) + w_i}}{e^{\beta(p + (1-p)\cos(\mu_{r,s}) + \|\mathbf{y}\|\cos(\mu_{r,s})) + w_i}}$$

And thus simplifying we have

$$\mathcal{S} \leq e^{\beta\{\cos(\mu_m) - \cos(\mu_{r,s})\}(1 + \|\mathbf{y}\|) - p + p\cos(\mu_{r,s}) + (w_i - w_r)}. \quad (11)$$

Note when $\log(\mathcal{S}) \ll 0$, we in particular have $\mathcal{S} \ll 1$. We will look at the logarithmic inequality corresponding to Eq. 11,

$$\log(\mathcal{S}) \leq \beta\{\cos(\mu_m) - \cos(\mu_{r,s})\}(1 + \|\mathbf{y}\|) - p + p\cos(\mu_{r,s}) + w_i - w_r.$$

To have a more explicit picture, let us consider an approximation for the angle between the isolated patterns, $\mu_{r,s}$, and for μ_m . Proceeding via a Taylor expansion, we have

$$\begin{aligned} \log(\mathcal{S}) &\leq \beta \left(\frac{\mu_{r,s}^2}{2} - \frac{\mu_m^2}{2} \right) (1 + \|\mathbf{y}\|) - \frac{p\mu_{r,s}^2}{2} + w_i - w_r + \mathcal{O}(\mu_{r,s}^4, \mu_m^4) \\ &\leq \beta \left(\frac{\mu_{r,s}^2}{2} - \frac{\mu_m^2}{2} \right) (1 + \|\mathbf{y}\|) + w_i - w_r + \mathcal{O}(\mu_{r,s}^4, \mu_m^4) \end{aligned}$$

Now, recall that we assumed that $\mu_{r,s} \ll \mu_m$. As such, for sufficiently large β (when $\beta\mu_{r,s}^2$ is of order unity, compared with w_i, w_r that are of order unity), we will expect to have $\log(\mathcal{S}) \ll 0$ and the non-isolated patterns do not contribute to the dynamics in the vicinity of Ξ^* .

D w-Modulation of the energy function and basins of attraction

In this section we explore how \mathbf{w} changes the energy landscape of our system. We aim to show that an increase in w_i leads to a decrease of the energy in the neighbourhood of Ξ_i , while leaving the energy around the other patterns virtually unchanged. As such we consider the symmetric case of $\mathbf{Q} = \Xi$, so that we have an energy function $V(\mathbf{x})$ given by Eq. 4. We focus on how the modulation of one component of \mathbf{w} , w_i , affects the energy landscape in the vicinity of our stable patterns.

To do this let us consider, how a small increase δ in w_i , affects the energy landscape. Let $\tilde{V}(\mathbf{x})$ be the modified energy landscape, i.e. one where $\tilde{w}_i = w_i + \delta$, then

$$\tilde{V}(\mathbf{x}) - V(\mathbf{x}) = \frac{1}{\beta}(\log(Z) - \log(\tilde{Z})) = \frac{1}{\beta} \left(\log \left(\frac{R + e^{\beta \Xi_i \cdot \mathbf{x} + w_i}}{R + e^{\beta \Xi_i \cdot \mathbf{x} + w_i + \delta}} \right) \right),$$

where $R = \sum_{j \neq i} e^{\beta \Xi_j \cdot \mathbf{x} + w_j}$. Considering the case where δ is small and doing a Taylor expansion we get

$$\tilde{V}(\mathbf{x}) - V(\mathbf{x}) = -\frac{e^{\beta \Xi_i \cdot \mathbf{x} + w_i}}{R + e^{\beta \Xi_i \cdot \mathbf{x} + w_i}} \delta + \mathcal{O}(\delta^2) = -s_i \delta + \mathcal{O}(\delta^2),$$

where s_i is the i^{th} component of the soft-max function. From this form, it is easy to see what a small increase in w_i will do to the energy landscape. Namely in the vicinity of Ξ_i , where $1 \approx s_i \gg s_j$, for all $j \neq i$, we get a significant decrease in the energy, while close to other patterns, where $s_i \approx 0$, the change in the energy will be negligible.

1 Estimation of the basins of attractions

In this section, we aim to derive a heuristic estimate for the basins of attractions. We aim to find the equations for the separatrices. Once again we assume that the dynamics arise from a potential function $V(\mathbf{x})$ given by Eqn. 4, so that $\mathbf{Q} = \Xi$.

D.1.1 Theoretical considerations

Assume we have a fixed point, p close to one of our patterns, Ξ_i say, i.e. it's the fixed point associated with Ξ_i . Suppose then we have a closed and convex region $\Omega \subseteq \mathbb{R}^N$, around p , and for all $\mathbf{x} \in \Omega$, $D^2V(\mathbf{x}) > 0$. Here $D^2V(\mathbf{x})$ is the Hessian of V at a point \mathbf{x} and by $D^2V(\mathbf{x}) > 0$ we mean that the Hessian is positive definite. Then the restriction of our potential to Ω , $V : \Omega \rightarrow \mathbb{R}$ is a strictly convex function. Therefore V has at most 1 minimum in Ω . So since our fixed point p is in Ω , p , will be a stable fixed point (as $D^2V(p) > 0$ by the assumption on Ω) and by the strict convexity it will be the only stable fixed point in Ω .

Now let us define the local sublevel sets of V on Ω to be $\Lambda(h)$, i.e. $\Lambda(h) := \{\mathbf{x} \in \Omega | V(\mathbf{x}) \leq h\}$. Note that this set is closed as V is continuous. Also considering V as a function from Ω to \mathbb{R} , which is convex by definition of Ω , we get that Λ_h is convex, as sublevel sets of a convex function are convex. Therefore as in our dynamical system, V is decreasing ($\dot{V} \leq 0$), Λ_h is an invariant-set, provided we chose h so that Λ_h is non-empty and $\Lambda_h \cap \partial\Omega = \emptyset$, where $\partial\Omega$ is the boundary of Ω . This implies that for Λ_h satisfying these properties, Λ_h is a subset of the basin of attraction of p , i.e. all trajectories starting in Λ_h will converge to p . Thus it will be imperative for us to be able to identify, when $D^2V > 0$.

D.1.2 Eigenvalues of the Hessian

A matrix is positive-definite if and only if all its eigenvalues are real and positive. As such our first task will be to compute the Hessian and figure out its eigenvalues. Note that we already know (from the dynamics of the system), that

$$\frac{\partial V(\mathbf{x})}{\partial x_i} = -(\Xi^T [\text{softmax}(\mathbf{w} + \beta \Xi \mathbf{x})])_i + x_i,$$

and as such by differentiating w.r.t x_j , we have

$$\frac{\partial^2 V(\mathbf{x})}{\partial x_i \partial x_j} = -\sum_{k=1}^K \xi_{ki} \left[\frac{\partial}{\partial x_j} \text{softmax}(\mathbf{w} + \beta \Xi \mathbf{x})_k + \delta_{ij} \right] = -\sum_{k=1}^K \xi_{ki} \left[\frac{\partial}{\partial x_j} \frac{e^{w_k + \beta \sum_{m=1}^N \xi_{km} x_m}}{Z} \right] + \delta_{ij},$$

where δ_{ij} is the Kronecker delta and Z is our partition function as before. Thus

$$\frac{\partial^2 V(\mathbf{x})}{\partial x_i \partial x_j} = -\sum_{k=1}^K \xi_{ki} \left[-\frac{e^{w_k + \beta \sum_{m=1}^N \xi_{km} x_m}}{Z^2} \frac{\partial Z}{\partial x_j} + \frac{e^{w_k + \beta \sum_{m=1}^N \xi_{km} x_m}}{Z} \beta \xi_{kj} \right] + \delta_{ij} \quad (12)$$

$$= -\sum_{k=1}^K \xi_{ki} \left[-\frac{s_k}{Z} \frac{\partial Z}{\partial x_j} + s_k \beta \xi_{kj} \right] + \delta_{ij}. \quad (13)$$

where s_k is the k^{th} component of our softmax function. Looking at the partition function we have

$$\frac{\partial Z}{\partial x_j} = \sum_{r=1}^K \frac{\partial}{\partial x_j} [e^{w_r + \beta \sum_{m=1}^N \xi_{rm} x_m}] = \sum_{r=1}^K [e^{w_r + \beta \sum_{m=1}^N \xi_{rm} x_m}] \beta \xi_{rj}.$$

Thus putting this back into Eq. 13, we have

$$\frac{\partial^2 V(\mathbf{x})}{\partial x_i \partial x_j} = - \sum_{k=1}^K \xi_{ki} [-s_k \beta \sum_{r=1}^K s_r \xi_{rj} + s_k \beta \xi_{kj}] + \delta_{ij} = -\beta \left[\sum_{k=1}^K \xi_{ki} s_k \xi_{kj} - \sum_{k=1}^K \sum_{r=1}^K \xi_{ki} s_k s_r \xi_{rj} \right] + \delta_{ij}.$$

The first term inside the square bracket corresponds to the ij^{th} component of $\Xi^T D_s \Xi$, where D_s is the diagonal matrix formed from the soft-max vector. While the second term corresponds to the ij^{th} entry of $\Xi^T (s \otimes s) \Xi$, where $s \otimes s$ refers to the outer product of the softmax with itself. Putting it all together, we thus have that

$$D^2 V(\mathbf{x}) = I - \beta \Xi^T (D_s - s \otimes s) \Xi = I - \beta \Xi^T J_s (\mathbf{w} + \beta \Xi \mathbf{x}) \Xi, \quad (14)$$

where J_s is the Jacobian of the softmax, i.e. $[J_s]_{ij} = \partial / \partial z_j [\text{softmax}(\mathbf{z})]$, which we evaluate at $\mathbf{z} = \mathbf{w} + \beta \Xi \mathbf{x}$. (Note that $J_s = D_s - s \otimes s$), and s is our softmax vector $s = \text{softmax}(\mathbf{w} + \beta \Xi \mathbf{x})$.

Note that as our potential $V(\mathbf{x})$ is a \mathcal{C}^2 function, it's Hessian matrix is symmetric, and as such all eigenvalues are real. Recall that if we have a positive-definite Hessian ($D^2 V > 0$) at a steady state, the steady state will be stable (as $\dot{\mathbf{x}} = -\nabla V(\mathbf{x})$) and if the Hessian is indefinite at a steady state, the steady state will be a saddle-point.

Now an equivalent condition for a symmetric matrix to be positive definite is that the minimal eigenvalue, λ_{\min} of the matrix is positive, i.e. $\lambda_{\min} > 0$. Now in general we cannot find the λ_{\min} explicitly for our Hessian, however we can find a subset of the regions, where the Hessian is positive-definite. Namely we have

Proposition D.1. *If $\lambda_{\max}(J_s)[\mathbf{x}] < \|\Xi\|_{op}^{-2} \beta^{-1}$ then $D^2 V(x) > 0$, where $\|\cdot\|_{op}$ is the operator norm² and $\lambda_{\max}(J_s)[\mathbf{x}]$, refers to the maximal eigenvalue of the Jacobian of the softmax evaluated at $\mathbf{z} = \mathbf{w} + \beta \Xi \mathbf{x}$.*

Proof. Now the Hessian is positive-definite iff $\lambda_{\min}(I - \beta \Xi^T J_s \Xi) > 0$. As I is an identity matrix, we can rewrite this condition as $1 + \lambda_{\min}(-\beta \Xi^T J_s \Xi) > 0$. From this we see that

$$\lambda_{\max}(\Xi^T J_s \Xi) < 1/\beta, \quad (15)$$

where we've employed the scaling of an eigenvalue and the fact that when we take out the minus sign, we change from a maximal to a minimal eigenvalue.

Recall that our matrix $\Xi^T J_s \Xi$ is real and symmetric, and so we may use the variational characterization of the maximal eigenvalue, namely for a real and symmetric matrix M , the maximal eigenvalue is given by the maximum over all vectors v of the quadratic form $(v^T M v) / (v^T v)$. As such we may rewrite Eq. 15 as

$$\max_{v \in \mathbb{R}^N} \left[\frac{v^T \Xi^T J_s \Xi v}{v^T v} \right] < \frac{1}{\beta}. \quad (16)$$

Now consider an arbitrary vector v , and let $z = \Xi v$, note that $\|z\| \leq \|\Xi\|_{op} \|v\|$, where $\|\cdot\|_{op}$, is the operator norm² of Ξ . Then we have

$$\frac{v^T \Xi^T J_s \Xi v}{v^T v} = \frac{z^T J_s z}{v^T v} = \frac{\|z\|^2}{\|v\|^2} \frac{z^T J_s z}{\|z\|^2} \leq \|\Xi\|_{op}^2 \frac{z^T J_s z}{\|z\|^2} \leq \|\Xi\|_{op}^2 \max_{z \in \mathbb{R}^K} \left[\frac{z^T J_s z}{\|z\|^2} \right] \quad (17)$$

Recall that $J_s = D_s - s \otimes s$ and thus in particular J_s is a real symmetric matrix, so that the variational description of the maximal eigenvalue is applicable to it. Thus by combining Eq. 16, Eq. 17 and the variational definition of the maximal eigenvalue we have

$$\frac{v^T \Xi^T J_s \Xi v}{v^T v} \leq \|\Xi\|_{op}^2 \lambda_{\max}(J_s).$$

Taking the maximum over $v \in \mathbb{R}^N$ we have that

$$\lambda_{\max}(\Xi^T J_s \Xi) < \|\Xi\|_{op}^2 \lambda_{\max}(J_s),$$

and as such we arrive at a sufficient condition for $D^2 V > 0$, namely $\lambda_{\max}(J_s) < \|\Xi\|_{op}^{-2} \beta^{-1}$. \square

From this proposition we see that when the maximal eigenvalue of the Jacobian of the softmax, J_s is smaller than $\|\Xi\|_{op}^{-2} \beta^{-1}$ then the Hessian of the energy functional $D^2 V$ is positive-definite. As such we proceeded to investigate the form of the eigenvalues of J_s . We do this by breaking it down into several propositions, for simplicity. The result for the maximal eigenvalue, which we are looking for is then presented in Proposition D.5.

Proposition D.2. $\forall \mathbf{x} \in \mathbb{R}^N, 0$ is always an eigenvalue of J_s .

²The operator norm of a linear operator, $A : V \rightarrow W$, where V, W are normed vector spaces, is defined as $\|A\|_{op} = \inf\{c : \|Av\|_W \leq c\|v\|_V\}$

Proof. To see this take the vector of 1's, in \mathbb{R}^K , which we denote by $\mathbf{1}$ i.e. $\mathbf{1} = (1, 1, \dots, 1)$. Then as $J_s = D_s - s \otimes s$, the i^{th} component of $J_s \mathbf{1}$ is

$$[J_s \mathbf{1}]_i = [D_s \mathbf{1}]_i - [(s \otimes s) \mathbf{1}]_i = s_i - \sum_{k=1}^K s_i s_k.$$

Now note that as the softmax is a probability vector, we have $\sum_k s_k = 1$ and thus

$$[J_s \mathbf{1}]_i = s_i - s_i = 0.$$

Hence $J_s \mathbf{1} = \mathbf{0}$ and 0 is an eigenvalue of J_s . \square

Now we proceed to derive an implicit equation for the eigenvalues in the specific case when the entries of the softmax are all different.

Proposition D.3. *The non-zero eigenvalues of $J_s[\mathbf{w} + \beta \Xi \mathbf{x}]$ are given by the solutions to the equation on the softmax entries*

$$\sum_{i=1}^K \frac{s_i}{s_i - \lambda} = 0, \quad (18)$$

where $s = (s_1, \dots, s_K)$, $s_i = [\text{softmax}(\mathbf{w} + \beta \Xi \mathbf{x})]_i$, provided for all i, j , such that $i \neq j$ we have $s_i \neq s_j$. (I.e. all the entries of the softmax are unique).

Proof. Take z an eigenvector and λ an eigenvalue of J_s . By definition we have that $D_s z - (s \otimes s)z = \lambda z$. Writing this in component form we have that,

$$s_i z_i - \sum_{k=1}^K s_i s_k z_k = \lambda z_i \quad \forall i \in \{1, \dots, K\}.$$

Now set $\bar{z} := \sum_k s_k z_k$, to get

$$(s_i - \lambda)z_i = s_i \bar{z} \quad \forall i \in \{1, \dots, K\}. \quad (19)$$

Summing over the i 's in Eq. 19, and recalling that as softmax is a probability vector, $\sum s_i = 1$, we get

$$\bar{z} - \lambda \sum z_i = \bar{z},$$

and as such either $\lambda = 0$, which we already know is an eigenvalue, or

$$\sum z_i = 0. \quad (20)$$

As we are in the non-zero eigenvalue case, we know that Eq. 20 holds. Now from Eq. 19 we also have that for a given $i \in \{1, \dots, K\}$ either $s_i = \lambda$ or $z_i = s_i \bar{z} / (s_i - \lambda)$.

Let us examine the first case with the i , for which $s_i = \lambda$, fixed. Now recall that in this proposition we are considering the case that $s_i \neq s_j$ for any $i \neq j$. As such for all $j \in \{1, \dots, K\} \setminus \{i\}$, $s_j \neq \lambda$. Now returning back to Eq. 19 for the i^{th} case and utilizing $s_i = \lambda$, we get $\bar{z} = 0$. But then for any other $j \neq i$, Eq. 19 gives

$$(s_j - \lambda)z_j = 0,$$

and as $s_j \neq \lambda$, $z_j = 0$. But then from Eq. 20, we must have that $z_i = 0$ and as such $z = 0$ and so cannot be an eigenvector.

As such we conclude that under the conditions of our propositions the second case must hold, and in fact it must hold for every $i \in \{1, \dots, K\}$ i.e.

$$z_i = \frac{s_i \bar{z}}{s_i - \lambda} \quad \forall i \in \{1, \dots, K\}.$$

Summing this equation over the i 's and by Eq. 20, we have that any eigenvalue must satisfy

$$\sum_{i=1}^K \frac{s_i \bar{z}}{s_i - \lambda} = 0,$$

and thus

$$\sum_{i=1}^K \frac{s_i}{s_i - \lambda} = 0.$$

Now to finish our proof, we only need to check that any solution of Eq. 18 is an eigenvalue. Hence suppose λ satisfies our equation and take a vector z to be given by $z_i = s_i / (s_i - \lambda)$. Then

$$[J_s z - \lambda z]_i = [D_s z - (s \otimes s)z - \lambda z]_i = \frac{s_i^2}{s_i - \lambda} - s_i \sum_{k=1}^K \frac{s_k^2}{s_k - \lambda} - \frac{\lambda s_i}{s_i - \lambda} = s_i \left(1 - \sum_{k=1}^K \frac{s_k^2}{s_k - \lambda} \right)$$

Therefore

$$[J_s z - \lambda z]_i = s_i \left(\sum_{k=1}^K s_k - \sum_{k=1}^K \frac{s_k^2}{s_k - \lambda} \right) = s_i \left(- \sum_{k=1}^K \frac{\lambda s_k}{s_k - \lambda} \right) = 0$$

and so λ is indeed an eigenvalue. \square

With this proposition, the only case left unexamined, is the case where some of the softmax entries are equal. This is precisely the subject of the following proposition.

Proposition D.4. *Suppose we have equal entries in the softmax. Denote them by $\sigma_1, \dots, \sigma_r$, i.e. for any m , σ_m is such that there exists some i, j ($i \neq j$) for which $s_i = s_j = \sigma_m$. (Note it can be the case that when more than 2 entries are equal, e.g. $s_1 = s_2 = s_3$, and we will still assign the same sigma to them, i.e. $\sigma_1 = s_1 = s_2 = s_3$ and so on for more identical entries.) Then the non-zero eigenvalues are given by the solutions of Eq 18 in Proposition D.3 and $\lambda_1 = \sigma_1, \dots, \lambda_r = \sigma_r$.*

Proof. We start by showing that any repeated entry is indeed an eigenvalue, $s_{i_1} = s_{i_2} = \dots = s_{i_M} =: \sigma$, for some collection of indices $\{i_1, \dots, i_M\}$, which we denote by \mathcal{I} . For our proof we will split our indices $\{1, \dots, K\}$ into those in \mathcal{I} and those not in \mathcal{I} .

We first look at the case when $\{1, \dots, K\} \setminus \mathcal{I} = \emptyset$, to illustrate the idea. In this scenario all entries of the softmax are equal and take the value σ . In this case take our candidate for eigenvector to be, $e_l - e_i$, where $i \neq l$ and e_i is one of the canonical basis vectors, i.e. the value of the j^{th} component is $[e_i]_j = \delta_{ij}$. By looking at the k^{th} component of the vector $[J_s(e_l - e_i)]_k = [(D_s - (s \otimes s))(e_l - e_i)]_k$, we have

$$[(D_s - (s \otimes s))(e_l - e_i)]_k = s_l \delta_{lk} - s_k \delta_{ik} - \sum_{m=1}^K s_k s_m \delta_{lm} + \sum_{m=1}^K s_k s_m \delta_{im} = \sigma \delta_{lk} - \sigma \delta_{ik} - \sigma^2 + \sigma^2.$$

As such we have

$$[(D_s - (s \otimes s))(e_l - e_i)]_k = \sigma \delta_{lk} - \sigma \delta_{ik} = \sigma [e_l - e_i]_k,$$

and we have that $J_s(e_l - e_i) = \sigma(e_l - e_i)$. Thus we have shown that σ is an eigenvalue of J_s (and in fact we've shown that it is the only non-zero eigenvalue, as $e_l - e_i$ span a $(K-1)$ -dimensional subspace).

Now we move onto the general case, suppose $\{1, \dots, K\} \setminus \mathcal{I} \neq \emptyset$. We denote by z , our candidate for our eigenvector and we take it to have the following form. We pick two arbitrary indices $a, b \in \mathcal{I}$. (Recall that by definition of \mathcal{I} , we must have $|\mathcal{I}| \geq 2$). Set

$$z_a = 1, z_b = -1 \text{ and } \forall (r \neq a, b) \text{ set } z_r = 0$$

Let us examine the vector $(D_s - (s \otimes s))z$ for our choice of z . Consider a component k . We have

$$[(D_s - (s \otimes s))z]_k = s_k z_k - \sum_{m=1}^K s_r s_m z_m = s_k (\delta_{ka} - \delta_{kb}) - s_k (s_a - s_b).$$

Proceeding further with the calculation we get

$$[(D_s - (s \otimes s))z]_k = s_k (\delta_{ka} - \delta_{kb}) - s_k (\sigma - \sigma).$$

where we have utilised the definition of σ . Now this gives us that for our choice of z , we get

$$J_s z = [D_s - (s \otimes s)]z = \sigma z,$$

where the last equality, crucially, follows from the fact that when $k \neq a, b$, ($\delta_{ka} = 0 = \delta_{kb}$) and when $k = a$ or $k = b$, $s_k = \sigma$. Thus z is indeed an eigenvector, with the eigenvalue σ . Note also that this eigenspace will be of dimension at least $|\mathcal{I}| - 1$, due to the free choices of a, b .

Finally, we need to show that the rest of the eigenvalues are given as before by the solutions to Eq. 18. We do this by the same calculation as in Proposition D.3. Let λ be a solution³ of Eq. 18. Take z to be a vector given by $z_i = s_i / (s_i - \lambda)$. By doing the exact same calculation as in Proposition D.3, we get

$$[J_s z - \lambda z]_i = [D_s z - (s \otimes s)z - \lambda z]_i = \frac{s_i^2}{s_i - \lambda} - s_i \sum_{k=1}^K \frac{s_k^2}{s_k - \lambda} - \frac{\lambda s_i}{s_i - \lambda} = s_i \left(1 - \sum_{k=1}^K \frac{s_k^2}{s_k - \lambda} \right)$$

Therefore

$$[J_s z - \lambda z]_i = s_i \left(\sum_{k=1}^K s_k - \sum_{k=1}^K \frac{s_k^2}{s_k - \lambda} \right) = s_i \left(- \sum_{k=1}^K \frac{\lambda s_k}{s_k - \lambda} \right) = 0$$

and so λ is indeed an eigenvalue. (Note also that λ has an eigenspace of dimension at least 1, and now summing over all the eigenspaces dimensions, we get that we have a complete characterization of the eigenvalues of J_s). \square

³Note that the only case when there are no solutions to the Eq. 18 is when all entries are equal

As such we can state the following about the maximal eigenvalue:

Proposition D.5. *The maximal eigenvalue of $J(s)$ is given by the maximal component of the soft-max, s_i , if there is another s_j such that $s_j = s_i$ and otherwise, it is given by the maximal solution of the equation*

$$\sum_{i=1}^K \frac{s_i}{s_i - \lambda} = 0. \quad (18)$$

D.1.3 Calculation of the estimated separatrix

We are interested in finding the separating surfaces, which form the boundaries between the basins of attractions and by above we expect that $\lambda_{\max}(J)$ can be used as a good estimate for this. To find the separatrix, we employ the following observation.

Consider the case when we are in a region where a single pattern Ξ_m is dominating the dynamics, i.e. $s_m \approx 1$. Then we can write for $j \neq m$, $s_j = \epsilon \rho_j$, where $\epsilon > 0$ is small and ρ_j is a rescaled variable, so that $\rho_j = \mathcal{O}(1)$. This then means $s_m = 1 - \epsilon(\sum_{j \neq m} \rho_j)$, and so Eq. 18 becomes

$$\frac{1 - \epsilon \sum_{j \neq m} \rho_j}{1 - \epsilon \sum_{j \neq m} \rho_j - \lambda(\epsilon)} + \sum_{j \neq m} \frac{\epsilon \rho_j}{\epsilon \rho_j - \lambda(\epsilon)} = 0,$$

where we have written $\lambda(\epsilon)$ to signify that λ is dependent on ϵ . Multiplying through to eliminate the fractions we get

$$(1 - \epsilon \sum_{j \neq m} \rho_j) \prod_{j \neq m} (\epsilon \rho_j - \lambda(\epsilon)) + (1 - \epsilon \sum_{j \neq m} \rho_j - \lambda(\epsilon)) \sum_{j \neq m} \epsilon \rho_j \prod_{k \neq j, m} (\epsilon \rho_k - \lambda(\epsilon)) = 0.$$

Employing an asymptotic expansion for $\lambda(\epsilon)$ of the form $\lambda(\epsilon) = \lambda_0 + \epsilon \lambda_1 + \mathcal{O}(\epsilon^2)$, we have

$$(1 - \epsilon \sum_{j \neq m} \rho_j) \prod_{j \neq m} (\epsilon \rho_j - \lambda_0 - \epsilon \lambda_1) + (1 - \epsilon \sum_{j \neq m} \rho_j - \lambda_0 - \epsilon \lambda_1) \sum_{j \neq m} \epsilon \rho_j \prod_{k \neq j, m} (\epsilon \rho_k - \lambda_0 - \epsilon \lambda_1) + \mathcal{O}(\epsilon^2) = 0.$$

Now focusing on the $\mathcal{O}(1)$ we get,

$$(-\lambda_0)^{K-1} = 0.$$

Therefore $\lambda_0 = 0$. So at a steady state we have $\lambda_{\max} \approx 0$.

Now imagine following a path $\pi(r)$ between two points p and q , parametrized by r so that $\pi(0) = p$ and $\pi(1) = q$. If p and q are two stable steady states, then considering $\lambda_{\max}(r)$ as a function of r , we have $\lambda_{\max}(0) \approx 0 \approx \lambda_{\max}(1)$. As between two stable steady states, there will necessarily be a separating surface, on that surface D^2V is not positive definite and hence in particular, $\lambda_{\max} > 1/\beta$. Moreover this means that $\lambda_{\max}(r)$ must have at least one turning point, and we will utilise it as our indicator of the position of the separatrix. As such we are interested in the points where

$$\frac{\partial \lambda_{\max}(r)}{\partial r} = 0$$

by the chain rule we get,

$$\frac{\partial \lambda_{\max}(r)}{\partial r} = \sum_{i=1}^K \frac{\partial \lambda_{\max}}{\partial s_i} \frac{\partial s_i}{\partial r}.$$

By differentiating Eq. 18, we have that λ_{\max} has to satisfy,

$$\frac{1}{s_i - \lambda_{\max}} - \frac{s_i}{(s_i - \lambda_{\max})^2} (1 - \frac{\partial \lambda_{\max}}{\partial s_i}) = 0,$$

and so $\frac{\lambda_{\max}}{s_i} = \frac{\partial \lambda_{\max}}{\partial s_i}$. Plugging this back in we have $\frac{\partial \lambda_{\max}(r)}{\partial r} = \lambda_{\max} \sum_{i=1}^K \frac{1}{s_i} \frac{\partial s_i}{\partial r}$. As such we will have a turning point when $\lambda_{\max} = 0$, which is the case when we are at a steady state or

$$0 = \sum_{i=1}^K \frac{1}{s_i} \frac{\partial s_i}{\partial r}.$$

Now recall that our position on the path \mathbf{x} is given by $\mathbf{x} = \pi(r)$. By differentiating the soft-max function we have

$$\frac{\partial s_i}{\partial r} = -\frac{e^{w_i + \sum_m \xi_{im} x_m}}{Z^2} \frac{\partial Z}{\partial r} + \frac{e^{w_i + \sum_m \xi_{im} x_m}}{Z} \beta \sum_m \xi_{im} \frac{\partial x_m}{\partial r},$$

and thus, by denoting $\pi_m(r)$ as the m^{th} co-ordinate of the path $\pi(r)$, we get

$$\frac{\partial s_i}{\partial r} = -\frac{s_i}{Z} \sum_j e^{w_j + \beta \sum_m \xi_{jm} x_m} \left(\beta \sum_m \xi_{jm} \frac{\partial \pi_m}{\partial r} \right) + s_i \beta \sum_m \xi_{im} \frac{\partial \pi_m}{\partial r},$$

and therefore we have

$$\begin{aligned} \frac{\partial s_i}{\partial r} &= -s_i \sum_j s_j \left(\beta \sum_m \xi_{jm} \frac{\partial \pi_m}{\partial r} \right) + s_i \beta \sum_m \xi_{im} \frac{\partial \pi_m}{\partial r}, \\ \frac{\partial s_i}{\partial r} &= \beta s_i \left[\sum_{m=1}^N \xi_{im} \frac{\partial \pi_m}{\partial r} - \sum_{j=1}^K \sum_{m=1}^N s_j \xi_{jm} \frac{\partial \pi_m}{\partial r} \right]. \end{aligned}$$

Rewriting this in terms of patterns Ξ_k , we get

$$\frac{\partial s_i}{\partial r} = \beta s_i \left[\Xi_i - \sum_{k=1}^K s_k \Xi_k \right] \cdot \frac{\partial \pi}{\partial r}.$$

Therefore the derivative of our maximal eigenvalue is given by

$$\frac{\partial \lambda_{\max}(r)}{\partial r} = \lambda_{\max} \beta \sum_{i=1}^K [(1 - K s_i) \Xi_i] \cdot \frac{\partial \pi}{\partial r}.$$

And so we have a turning point, and thus we predict a separatrix when

$$0 = \sum_{i=1}^K [(1 - K s_i) \Xi_i] \cdot \frac{\partial \pi}{\partial r}. \quad (21)$$

We note that when $\pi(r)$ is just a straight line between p and q , we have

$$0 = \sum_{i=1}^K [(1 - K s_i) \Xi_i] \cdot (p - q). \quad (22)$$

2 Separatrix between two patterns

In this subsection we aim to derive the equation approximating the separatrix, between two patterns. Suppose we have two patterns Ξ_i, Ξ_k , with the angle between them being $\angle(\Xi_i, \Xi_k) = \mu$ (note that this will also be the relevant effective dynamics when the softmax entries of the other patterns are small). Further let us assume that β is such that the bifurcation separating Ξ_i from Ξ_k occurred. As before we assume that the patterns have norm unity. From Eq. 22, we predict that a point on our separatrix must satisfy

$$0 = [(1 - 2s_i) \Xi_i + (1 - 2s_k) \Xi_k] \cdot (p - q).$$

And so $0 = [(s_k - s_i) \Xi_i + (s_i - s_k) \Xi_k] \cdot (p - q) = (s_k - s_i) (\Xi_i - \Xi_k) \cdot (p - q)$. Therefore provided Ξ_i and Ξ_k are linearly independent, we have that $s_i = s_k$ and so our estimate for the separatrix equation is

$$w_i + \beta \Xi_i \cdot \mathbf{x} = w_k + \beta \Xi_k \cdot \mathbf{x}$$

As such we get that any point on the separatrix must satisfy $\mathbf{x} \cdot (\Xi_i - \Xi_k) = -(w_i - w_k)/\beta$, which we recognize as an equation for a hyperplane.

To see how far from the mid-point between two patterns the separatrix, we look at $\mathbf{x} = (\Xi_i + \Xi_k)/2 + r(\Xi_i - \Xi_k)$, i.e. the straight line connecting the two patterns, we find that:

$$r \|\Xi_i - \Xi_k\|^2 = -\frac{w_i - w_k}{\beta}$$

and so

$$r = -\frac{w_i - w_k}{\beta(2 - 2\cos(\mu))}$$

Therefore the offset from the middle point between two patterns ($(\Xi_i + \Xi_k)/2$) will be given by

$$\Delta = \frac{(w_i - w_k) \|\Xi_i - \Xi_k\|}{\beta(2 - 2\cos(\mu))}.$$

Finally note that when we only have two patterns we may write $\Xi_i = (\cos(\mu/2), \sin(\mu/2))$, $\Xi_k = (\cos(\mu/2), -\sin(\mu/2))$ and thus

$$\Delta = \frac{(w_i - w_k) \sin(\mu/2)}{\beta(1 - \cos(\mu))}, \quad (23)$$

where the offset moves the separatrix Δ closer to Ξ_k . A comparison between our analytical prediction and numerical results, and an illustration of the w-modulated offset can be seen in Figure 2.

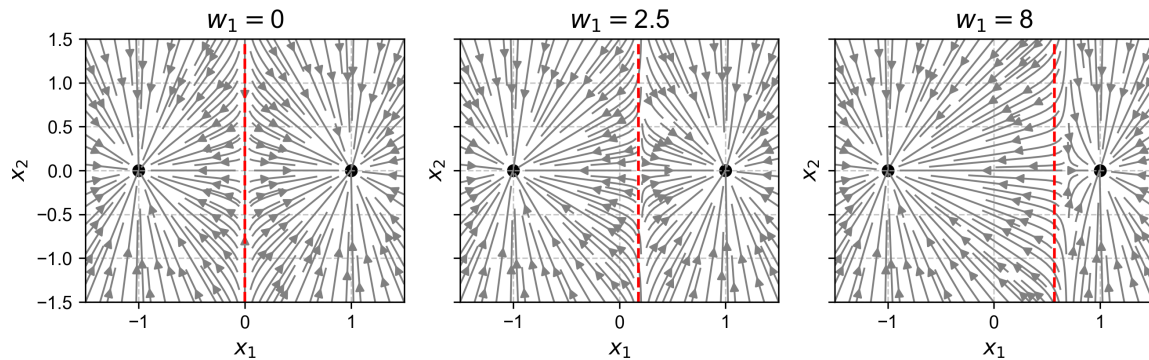


Figure 2: An example of how modulating w_1 moves the separatrix between two patterns In this example we have 2 patterns, represented by black dots. Ξ_1 is the pattern on the left. The red dashed line represents the analytic estimate for the separatrix. In this simulation $\beta = 7$, $\mathbf{w} = (w_1, 0)$.

D.2.1 Effect of a far away pattern on the separatrix

In this section, we will show that an addition of a pattern that is far away from the two patterns doesn't affect the position of the separatrix between the two close patterns. In this section we suppose that all patterns are of unit magnitude. Consider then two isolated patterns, Ξ_i, Ξ_k , with an angle μ between them and a pattern far away, Ξ_r , say. As in section C, we suppose that $\mu \ll \angle(\Xi_i, \Xi_r), \angle(\Xi_k, \Xi_r)$. We further suppose that β is large enough so that the bifurcation separating Ξ_i and Ξ_k occurred.

To see this let us consider our separatrix equation given by Eq. 22, when π is just a straight line between $p = \Xi_i$ and $q = \Xi_k$, i.e. we are looking at the straight line between the two patterns. We have

$$0 = \sum_{m=1}^K [(1 - K s_m) \Xi_m] \cdot (\Xi_i - \Xi_k).$$

As $K = 3$, in our case, expanding we get

$$0 = [(1 - 3s_i)\Xi_i + (1 - 3s_k)\Xi_k + (1 - 3s_r)\Xi_r] \cdot (\Xi_i - \Xi_k).$$

Now as our patterns have a unity magnitude, we get

$$0 = (1 - 3s_i)(1 - \cos(\mu)) + (1 - 3s_k)(\cos(\mu) - 1) + (1 - 3s_r)(\cos(\angle(\Xi_i, \Xi_r)) - \cos(\angle(\Xi_k, \Xi_r))),$$

and so simplifying we have

$$0 = 3(s_k - s_i)(1 - \cos(\mu)) + (1 - 3s_r)(\cos(\angle(\Xi_i, \Xi_r)) - \cos(\angle(\Xi_k, \Xi_r))). \quad (24)$$

Now as Ξ_r is the isolated pattern, we will have that $\angle(\Xi_i, \Xi_r) \approx \angle(\Xi_k, \Xi_r)$ and thus Eq. 24 becomes

$$0 \approx 3(s_k - s_i)(1 - \cos(\mu)),$$

and so $s_k = s_i$, and the position of the separatrix is thus the same as in the case where we only considered two patterns.

3 Control of progenitor basins by modulation of \mathbf{w}

Consider now modulating one component of \mathbf{w} , w_i . And suppose we coarse-grain the patterns with the indices given by \mathcal{L} such that, $i \in \mathcal{L}$. Then comparing the separatrix between the coarse-grained pattern, Ξ^* and another pattern Ξ_r , we have from Eq. 23 that the offset from the separatrix is given by

$$\Delta = \frac{(w^* - w_k) \sin(\mu/2)}{\beta(1 - \cos(\mu))} = \frac{(\log(\sum_{j \in \mathcal{L}} e^{w_j}) - w_k) \sin(\mu/2)}{\beta(1 - \cos(\mu))},$$

where μ is the angle between Ξ^* and Ξ_k . Note that we have the following bounds on $\log(\sum_{j \in \mathcal{L}} e^{w_j})$, namely

$$\max_{j \in \mathcal{L}}(w_j) \leq \log(\sum_{j \in \mathcal{L}} e^{w_j}) \leq \max_{j \in \mathcal{L}}(w_j) + \log(|\mathcal{L}|)$$

Now consider increasing w_i , starting from 0, we see that while $w_i < \max_{j \in \mathcal{L}}(w_j)$, it makes negligible contribution to the position of the separatrix of the progenitor pattern. However once $w_i = \max(w_j)$, then it is the main contributor to the position of the separatrix and we have that

$$\Delta \geq \frac{(w_i - w_k) \sin(\mu/2)}{\beta(1 - \cos(\mu))}.$$

This is precisely what we see in our simulations. We present an example of the modulation of the separatrix of the coarse-grained pattern by \mathbf{w} in Figure 3.

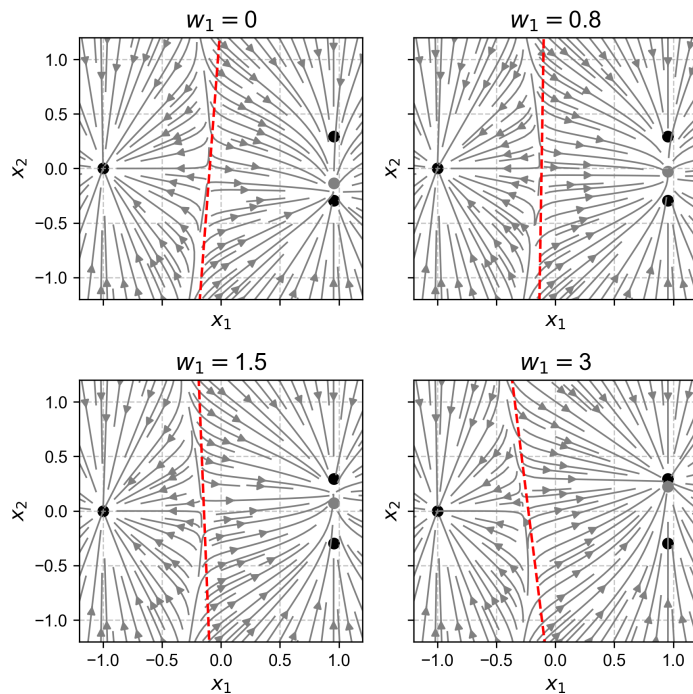


Figure 3: An example of how modulating w_1 moves the separatrix of the coarse-grained pattern In this example we have 3 patterns, represented by black dots, with a coarse-grained pattern (gray dot), stemming from Ξ_1 and Ξ_2 . Ξ_1 is the upper right pattern. The red dashed line represents the analytic estimate for the separatrix. In this simulation $\beta = 7$, $\mathbf{w} = (w_1, 1, 0)$. As seen w_1 has little effect on the position of the separatrix until $w_1 > w_2 = 1$.

E Local instability and the calculation of β_{crit} for equal-angle patterns

Consider a set of K patterns Ξ of dimension N for which each pattern is of magnitude unity and at angle μ relative to all other patterns. Furthermore we assume that $\mathbf{w} = 0$. As per Section B, since the dynamics are rotationally invariant, we can assume, without loss of generality, that these patterns are given by *any* K dimensional set of vectors for which:

$$\Xi_i \cdot \Xi_j = \begin{cases} \cos \mu & \text{if } i \neq j \\ 1 & \text{if } i = j \end{cases} \quad (25)$$

as an example, in two dimensions, we have that:

$$\Xi_1 = (1, 0), \quad \Xi_2 = (\cos \mu, \sin \mu) \quad (26)$$

while in three dimensions, we have that

$$\Xi_1 = (1, 0, 0), \quad \Xi_2 = (\cos \mu, \sin \mu, 0), \quad \Xi_3 = \left(\cos \mu, \cos \mu \tan\left(\frac{\mu}{2}\right), \sqrt{(2 \cos \mu + 1) \tan^2\left(\frac{\mu}{2}\right)} \right) \quad (27)$$

we further assume that the weights are all identical, and thus the system is entirely symmetric. In this case, our "progenitor" state corresponds to:

$$\Xi^* = \frac{1}{K} \sum_i \Xi_i \quad (28)$$

What is the stability of Ξ^* ? We can address this by linear stability analysis, by estimating the Jacobian of Eq. 1 around $\mathbf{x} = \Xi^*$. Since the dynamics are associated with a potential function (symmetric Jacobian) the eigenvalues are real at any evaluated point, and Ξ^* may be a stable fixed point only if all its associated eigenvalues are negative. For two equidistant patterns, these eigenvalues are given by $\lambda_{1,2} = -1, \frac{1}{2}(\beta(1 - \cos \mu) - 2)$, and there is thus a bifurcation at $\beta(1 - \cos \mu) = 2$ (that is, around $\beta\mu^2 = 4$). For three patterns, the eigenvalues are $\lambda_{1,2,3} = -1, \frac{1}{3}(\beta(1 - \cos \mu) - 3), \frac{1}{3}(\beta(1 - \cos \mu) - 3)$, and the bifurcation occurs at around $\beta(1 - \cos \mu) = 3$. Similarly, for K patterns, we expect the bifurcation to occur at the critical $\beta(1 - \cos \mu) = K$, which we indeed verify numerically. Thus, a transition from progenitor to terminal pattern, for an isolated subset of K patterns, occurs at a critical $\beta_{\text{crit}} \approx 2K\mu^{-2}$.

In fact we can analytically derive the critical value of β , β_{crit} for which the bifurcation occurs. The rest of this section is dedicated to showing this result.

Proposition E.1. *For K patterns, with all having an angle μ between each other, as above, all the eigenvalues of the Jacobian of Eq. 1 evaluated at $\mathbf{x} = \Xi^*$ are negative, provided*

$$\beta(1 - \cos(\mu)) < K,$$

and $\cos(\mu) \neq -1/(K - 1)$.

To prove this we will utilise the following lemma.

Lemma E.2. *If a collection of patterns Ξ_1, \dots, Ξ_K , satisfy Eq. 25, then provided*

$$\cos(\mu) \neq -\frac{1}{(K - 1)}$$

holds, the collection of patterns is linearly independent.

Proof. Consider the equation $c_1\Xi_1 + \dots + c_K\Xi_K = 0$, by looking at the inner product with Ξ_i , we have from Eq. 25

$$1 + \sum_{j \neq i} c_j \cos(\mu) = 0.$$

Now let $c = \sum_{j=1}^K c_j$, then our equation becomes

$$c_i + (c - c_i) \cos(\mu) = 0. \tag{29}$$

Note that this is true for all $i \in \{1, \dots, K\}$, so summing over the indices we have $c + (Kc - c) \cos(\mu) = 0$, and so

$$c(1 + (K - 1) \cos(\mu)) = 0.$$

Thus we must have either $c = 0$ or $\cos(\mu) = -1/(K - 1)$ and the second case is excluded due to our assumption. So we have $c = 0$ and so plugging this into Eq. 29, we get

$$c_i(1 - \cos(\mu)) = 0.$$

As $\cos(\mu) = 1$ implies $\mu = 0$ (i.e. there is no angle between patterns and so there is only one pattern), and we have $\mu > 0$, we conclude that $c_i = 0$ and so our patterns are linearly independent. \square

We remark that the case that is excluded from the lemma above, namely $\cos(\mu) = -1/(K - 1)$ cannot give linear independence. In that case $\Xi^* = 0$ and so we have a linear dependence of patterns⁴. With the lemma in mind we return back to the proof of Proposition E.1.

Proof of Proposition E.1. We are interested in the stability of the progenitor pattern

$$\Xi^* = \frac{1}{K} \sum_{i=1}^K \Xi_i.$$

Recall that we are working in the case, when $\mathbf{Q} = \Xi$, and so we have an energy functional given by Eq. 4. In this case, we know that the Hessian of the energy function (which is the negative of the Jacobian of the dynamics) is given by Eq. 14, i.e.

$$D^2V(\mathbf{x}) = I - \beta\Xi^T J_s(\mathbf{w} + \beta\Xi\mathbf{x})\Xi.$$

Now recall that we are assuming $\mathbf{w} = \mathbf{0}$ and we are interested at $\mathbf{x} = \Xi^*$. Looking then at the i^{th} component of the softmax we have

$$[\text{softmax}(\mathbf{w} + \beta\Xi\mathbf{x})]_i = \frac{e^{\beta\Xi_i \cdot \Xi^*}}{Z} = \frac{e^{\beta(1 + \cos(\mu)(K-1)/K)}}{Z}.$$

⁴However as mentioned previously, as we're in the symmetric case of $\Xi = \mathbf{Q}$, our singular value decomposition would give 0 as one of the singular values, as we've just seen that in this case the rank of Ξ is $K - 1$, and we could further reduce the dimension of our problem by one

In particular this shows that all the components of the softmax are equal at $\mathbf{x} = \Xi^*$ and thus as it is a probability vector

$$[\text{softmax}(\mathbf{w} + \beta \Xi \mathbf{x})]_i = \frac{1}{K}. \quad (30)$$

Note that the eigenvalues of a real symmetric matrix are all positive if and only if the minimal eigenvalue is positive. Thus, as in Section D, we employ a variational characterisation of the maximal eigenvalue, i.e. the eigenvalues of the Jacobian of our dynamics at Ξ^* are all negative (meaning the Hessian of the energy is positive definite) if and only if Eq. 16 holds at $\mathbf{x} = \Xi^*$, namely

$$\max_{v \in \mathbb{R}^K} \left[\frac{v^T \Xi^T J_s \Xi v}{v^T v} \right] < \frac{1}{\beta},$$

which is equivalent to the condition

$$\max_{v \in \mathbb{R}^K, \|v\|=1} [v^T \Xi^T J_s \Xi v] < \frac{1}{\beta}, \quad (31)$$

so now throughout we will assume $\|v\| = 1$. If we set $u = \Xi v$, we have

$$v^T \Xi^T J_s \Xi v = u^T J_s u = u^T (D_s - s \otimes s) u = \sum_{r=1}^K u_r^2 s_r - \left(\sum_{r=1}^K u_r s_r \right)^2,$$

where s_i is the i^{th} component of the softmax at $\mathbf{x} = \Xi^*$. Now by Eq. 30 we get

$$v^T \Xi^T J_s \Xi v = \frac{1}{K} \sum_{r=1}^K u_r^2 - \frac{1}{K^2} \left(\sum_{r=1}^K u_r \right)^2. \quad (32)$$

Now utilising the assumption that $\cos(\mu) \neq -1/(K-1)$, we have by Lemma E.2 that Ξ_1, \dots, Ξ_K are linear independent, and thus form a basis (as we have K dimensional vector space) so we may write

$$v = \sum_{m=1}^K \alpha_m \Xi_m,$$

and so

$$u_i = [\Xi v]_i = \Xi_i \cdot v = \sum_{m=1}^K \alpha_m \Xi_i \cdot \Xi_m = \alpha_i + \cos(\mu) \sum_{m \neq i} \alpha_m = \alpha_i + \cos(\mu)(A - \alpha_i),$$

where $A = \sum_{m=1}^K \alpha_i$. Plugging this back into Eq. 32, we have

$$v^T \Xi^T J_s \Xi v = \frac{1}{K} \sum_{r=1}^K (\alpha_r + \cos(\mu)(A - \alpha_r))^2 - \frac{1}{K^2} \left(\sum_{r=1}^K (\alpha_r + \cos(\mu)(A - \alpha_r)) \right)^2.$$

So setting $S = \sum_{m=1}^K \alpha_m^2$, and expanding we have

$$v^T \Xi^T J_s \Xi v = \frac{1}{K} \sum_{r=1}^K [\alpha_r^2 + 2\alpha_r \cos(\mu)(A - \alpha_r) + \cos^2(\mu)(A - \alpha_r)^2] - \frac{1}{K^2} [A + \cos(\mu)(AK - A)]^2,$$

and thus

$$v^T \Xi^T J_s \Xi v = \frac{1}{K} [S + 2 \cos(\mu)(A^2 - S) + \cos^2(\mu)(A^2 K - 2A^2 + S)] - \frac{1}{K^2} [A + \cos(\mu)A(K-1)]^2.$$

Expanding further and simplifying we get

$$v^T \Xi^T J_s \Xi v = \frac{1}{K} [S(1 - 2 \cos(\mu) + \cos(\mu)^2) + A^2 K \cos^2(\mu)] - \frac{A^2}{K^2} [1 + (K-1) \cos(\mu)]^2,$$

giving

$$v^T \Xi^T J_s \Xi v = \frac{1}{K} [S(1 - \cos(\mu))^2 + A^2 K \cos^2(\mu)] - \frac{A^2}{K^2} [1 + (K-1) \cos(\mu)]^2. \quad (33)$$

Before proceeding further with this calculation, recall that we are interested in the vectors such that $\|v\| = 1$ and thus

$$1 = \|v\|^2 = v \cdot v = \left(\sum_{l=1}^K \alpha_l \Xi_l \right) \cdot \left(\sum_{m=1}^K \alpha_m \Xi_m \right) = \sum_{l=1}^K \sum_{m=1}^K \alpha_l \alpha_m \Xi_l \cdot \Xi_m.$$

Thus

$$1 = \sum_{l=1}^K \left(\alpha_l^2 + \alpha_l \sum_{m \neq l}^K \alpha_m \cos(\mu) \right) = S + \sum_{l=1}^K \alpha_l \cos(\mu) (A - \alpha_l) = S + \cos(\mu) (A^2 - S).$$

And as such we have

$$S = \frac{1 - A^2 \cos(\mu)}{1 - \cos(\mu)}.$$

Plugging this back into Eq. 33,

$$v^T \Xi^T J_s \Xi v = \frac{1}{K} [(1 - A^2 \cos(\mu))(1 - \cos(\mu)) + A^2 K \cos^2(\mu)] - \frac{A^2}{K^2} [1 + (K - 1) \cos(\mu)]^2.$$

Simplifying this we get

$$\begin{aligned} v^T \Xi^T J_s \Xi v &= \frac{1}{K} [(1 - A^2 \cos(\mu))(1 - \cos(\mu))] + A^2 \cos^2(\mu) - \frac{A^2}{K^2} [1 + (K - 1) \cos(\mu)]^2, \\ &= \frac{1}{K} [(1 - A^2 \cos(\mu))(1 - \cos(\mu))] + \frac{A^2}{K^2} [K^2 \cos^2(\mu) - 1 + 2(K - 1) \cos(\mu) - (K - 1)^2 \cos(\mu)^2], \\ &= \frac{(1 - \cos(\mu))}{K} - \frac{(A^2 \cos(\mu))(1 - \cos(\mu))}{K} + \frac{A^2}{K^2} [-1 + 2(K - 1) \cos(\mu) + (2K - 1) \cos(\mu)^2], \\ &= \frac{(1 - \cos(\mu))}{K} + \frac{A^2}{K^2} [-1 + (K - 2) \cos(\mu) + (3K - 1) \cos(\mu)^2]. \end{aligned}$$

Recall that by Eq. 31 we want to maximise $v^T \Xi^T J_s \Xi v$ and as such, since A is the only variable at play, this is achieved when $\partial(v^T \Xi^T J_s \Xi v) / \partial A = 0$, i.e. precisely when $A = 0$, and thus condition(31) now gives

$$\frac{1 - \cos(\mu)}{K} < \frac{1}{\beta}.$$

Therefore whenever this condition holds, the maximal eigenvalue of the Jacobian of our dynamics is negative, and hence all eigenvalues are negative. \square

From this proposition we deuce that when $K = \beta(1 - \cos(\mu))$, one of the eigenvalues of the Jacobian of the dynamics, becomes zero. Hence we get a change in the dynamical behaviour and thus a bifurcation.

F Model for cell identity regulation

1 General model for gene regulatory network based on enhancer selection

For completeness, we include here the derivation of the model for cell identity regulation that has been first derived in Karin [1]. The idea behind the model is as follows. Cell identity is determined by the expression of DNA-binding proteins called transcription factors (TFs). We associate each TF with an expression level x_j , corresponding to protein concentration in the cell (we can, more generally, consider the expression level of *any* protein in the cell). The expression level x_j is determined by the rate of transcription initiation from the gene, which is, in turn, determined by recruitment of rate-limiting transcriptional machinery such as RNA polymerase molecules and other transcription initiation factors [2]. This recruitment occurs through enhancers, which are genomic regions associated with TF binding, and which can initiate transcription from nearby or remote genes. Within our mathematical framework, each enhancer is associated with a binding profile for TFs $\xi_{i,1}, \dots, \xi_{i,N}$. Since an enhancer can, in principle, initiate transcription in more than a single gene, we will assume that, upon recruitment of transcription initiation machinery to the enhancer, transcription can be initiated in genes by the rates $q_{i,1}, \dots, q_{i,N}$. The expression level of x_j is thus given by:

$$\dot{x}_j = \sum_{i=1}^K q_{i,j} p_i - x_j$$

where time is rescaled to unity, and with p_i representing the rate of recruitment of transcription initiation machinery to enhancer i . We will assume that, on the timescale of cell identity changes, p_i can be captured by an equilibrium (Boltzmann) distribution

$$p_i = \frac{e^{-\epsilon_i}}{\sum_{k=1}^K e^{-\epsilon_k}}$$

with ϵ_i corresponding to the energy associated with transcription initiation from enhancer i . This energy is, in turn, set by the chromatin state of the enhancer, such as the level of histone acetylation [2, 3], which we denote

m_i . This is modulated by the recruitment of co-factors such as p300 by transcription factors, and, thus, its dynamics are captured by

$$\dot{m}_i = \kappa_1 \sum_{j=1}^N \xi_{i,j} x_j - \kappa_{-1} m_i$$

where κ_1 and κ_{-1} are the corresponding forward and backward rates which may be controlled by the cell through, for example, adjusting the abundances of relevant enzymes. The energy is determined by:

$$\epsilon_i = -m_i - w_i$$

with w_i providing the baseline energy of the enhancer (it also captures any upstream enhancer modulation, such as due to signalling). Since the dynamics of histone acetylation appear to be fast (minutes-hours) relative to the timescale of cell identity changes (hours-weeks) [2], we take a quasi-steady-state approximation on m_i and thus we have that:

$$m_i = \beta \Xi_i \cdot \mathbf{x} \quad (34)$$

with $\beta = \kappa_1/\kappa_{-1}$. Putting this all together, we recreate equation 1.

2 Symmetric dynamics derived from autoregulatory dynamics

A recurring motif, across dozens of cell types, is autoregulation, where specific sets of TFs co-bind adjacent enhancers [4]. Within our modelling framework, such a motif corresponds to a set \mathcal{L} such that for $i \in \mathcal{L}$, we have that $\Xi_i = \mathbf{z}$ where \mathbf{z} has large positive entries for all $i \in \mathcal{L}$ and zero entries for $i \notin \mathcal{L}$; and that Q_i has a large positive entry at index i and zero otherwise. Coarse-graining on \mathcal{L} , which is associated with identical memory patterns, leaves the dynamics invariant; and its associated coarse-grained patterns are $\Xi_{\mathcal{L}}^* = \mathbf{z}$ and $Q_{\mathcal{L}}^* \approx \mathbf{z}$ since it is averaged of all Q_i . Thus, the effective dynamics of the cell identity network approximates the symmetric dynamics of Eq. 4.

3 Simulation of annealing in blood production

Data preparation of gene expression profiles of haematopoietic lineages was based on mouse RNA sequencing data from Haemopedia [5] and preprocessed as in Karin [1]. Annealing was executed as follows. The dynamics were given by the noisy version of Eq. 1:

$$d\mathbf{x} = (\Xi^T \text{softmax}(\beta \Xi \mathbf{x} + \mathbf{w}) - \mathbf{x}) dt + \sigma dW, \quad (35)$$

where W is a Wiener process and σ corresponds to the noise magnitude (set to $\sigma = 0.05$). Simulation was performed using the Euler-Maruyama procedure. Annealing was performed with initial conditions as $\mathbf{x}(0) = \text{softmax}(\mathbf{w}) + \zeta$ where ζ is a random vector of length N with entries drawn from a uniform distribution over $[0, 0.1]$. Annealing itself was executed by a gradual increase of β from $\beta = 0$ to $\beta = 50$ over $t = 20$ time units.

To estimate \mathbf{w} for balanced differentiation, we used proportional feedback, namely, after each annealing iteration (performed over $n = 1000$ cellular instances), we calculated the error vector:

$$\text{err} = \mathbf{1} - K\rho \quad (36)$$

where ρ is a K dimensional vector (with an entry for each cell type) with its i -th entry corresponding to the relative prevalence of cell type i in the annealing output. Note that a perfectly balanced annealing process would produce $\text{err} = \mathbf{0}$; and that the control process can be adjusted to produce any output range by replacing $\mathbf{1}$ in Eq. 36 by the desired output profile. The error was then fed to \mathbf{w} by the feedback procedure: $\mathbf{w}(t+1) \leftarrow \mathbf{w}(t) + G_p \text{err}$ with G_p denoting the feedback gain. In our simulations, the procedure was executed by running 100 iterations at gain $G_p = 0.1$, followed by 100 iterations at $G_p = 0.01$ and 100 iterations at $G_p = 0.001$.

References

- [1] Omer Karin. Enhancernet: A predictive model of cell identity dynamics through enhancer selection. *Development*, 151(19):dev202997, 2024.
- [2] Takeo Narita, Shinsuke Ito, Yoshiki Higashijima, Wai Kit Chu, Katrin Neumann, Jonas Walter, Shankha Satpathy, Tim Liebner, William B Hamilton, Elina Maskey, et al. Enhancers are activated by p300/cbp activity-dependent pic assembly, rnapii recruitment, and pause release. *Molecular Cell*, 81(10):2166–2182, 2021.
- [3] Denes Hnisz, Brian J Abraham, Tong Ihn Lee, Ashley Lau, Violaine Saint-André, Alla A Sigova, Heather A Hoke, and Richard A Young. Super-enhancers in the control of cell identity and disease. *Cell*, 155(4):934–947, 2013.

-
- [4] Violaine Saint-André, Alexander J Federation, Charles Y Lin, Brian J Abraham, Jessica Reddy, Tong Ihn Lee, James E Bradner, and Richard A Young. Models of human core transcriptional regulatory circuitries. *Genome research*, 26(3):385–396, 2016.
- [5] Jarny Choi, Tracey M Baldwin, Mae Wong, Jessica E Bolden, Kirsten A Fairfax, Erin C Lucas, Rebecca Cole, Christine Biben, Clare Morgan, Kerry A Ramsay, et al. Haemopedia rna-seq: a database of gene expression during haematopoiesis in mice and humans. *Nucleic acids research*, 47(D1):D780–D785, 2019.